Japan). Mice were housed under climate-controlled conditions with a 12-hour light/dark cycle and were provided with standard food and water ad libitum as described previously.[12] All protocols were approved by the Institutional Animal Care and Use Committee of Chiba University.

MI Model

MI was produced in male WT and AT1KO mice by left coronary artery ligation as described previously.[4] Mice were sacrificed at 1, 4, 7, and 14 days after the operation. Sham-operated control mice did not receive coronary artery ligation. Before procedure, systolic blood pressure (SBP) and heart rate were measured by using a tail-cuff method.[12]

Hydralazine Treatment

It has been reported that SBP was lower in AT1KO mice than WT mice.[11,13] To examine the effect of BP on angiogenesis, we administered hydralazine (Norvartis Pharmaceuticals, Tokyo, Japan) to WT mice. WT mice were treated with hydralazine (3 mg/kg per day) through osmotic mini pump (Alzet, Palo Alto, Calif)[14] from 1 week before procedure to euthanization. Our preliminary experiments showed that SBP in WT mice treated with this dose of hydralazine was similar to that in AT1KO mice.

Number of Capillaries and Arterioles

We examined neovascularization by measuring the number of capillaries and arterioles in light microscopic sections taken from the border zone of the infarcted heart. Capillary endothelial cells and smooth muscle α-actin (SMA) were identified by immunohistochemical staining with anti-platelet/endothelial cell adhesion molecule (PECAM) antibody and anti-SMA antibody (PROGEN Biotechnik GmbH, Heidelberg, Germany), respectively. Ten random microscopic fields were examined and the number of capillaries and arterioles were expressed as the number of PECAM-positive capillaries and SMA-positive arteriole/high-power field (HPF) (×400).[7]

Histological Analysis for Inflammatory Response

Immunohistochemical analysis was performed with anti-Ly6G antibody, anti-Mac3 antibody, and anti-CD3 antibody (BD Pharmingen, San Diego, Calif) to detect granulocytes, macrophages, and T lymphocytes, respectively, according to the supplier's instructions. We counted positive cells in 10 random microscopic HPFs.

Western Blot Analysis

Protein extracts were obtained after homogenization of infarcted myocardium; 100 μg of protein was separated on a polyacrylamide gel and electroblotted onto nitrocellulose transfer membrane (Schleicher & Schuell, Dassel, Germany). The membrane was blocked with 5% skim milk and 0.5% BSA in PBS with 0.1% Tween-20 (T-PBS) and then probed with anti-matrix metalloproteinase (MMP)-2 antibody, anti- MMP-9 antibody, anti-Akt antibody, anti-endothelial nitric oxide synthase (eNOS) antibody, and anti-phospho-Akt antibody (Cell Signaling, Beverly, Mass) for 1 hour at room temperature. After incubation with the primary antibody, the membrane was washed in T-PBS and was incubated for 1 hour with peroxidase-conjugated secondary antibody. The reaction was detected using ECL detection reagent kit (Amersham Pharmacia, Buckinghamshire, UK).

NOS Activity Assay and NOS Inhibition

The NOS activity (calcium-dependent) in infarcted myocardium was examined using NOS assay kit (Calbiochem, San Diego, Calif) according to the manufacture's instruction. To examine the role of eNOS in angiogenesis after MI, we administered a NOS inhibitor, N^G-nitro-L-arginine methyl ester (L-NAME) (4 mg/kg per day) via drinking water to WT mice from 1 week before procedure to euthanization.

Ribonuclease Protection Assay

Total RNA was extracted from left ventricles with RNAzol B (Biotecx Laboratories) and analyzed by ribonuclease protection assay. Multi-probes template sets, mCK-3b and mCK-5, were available with reagents of in vitro transcription and ribonuclease protection assay (RiboQuant; Pharmingen). For all hybridization assays, we used 2 μg total RNA from the sham-operated mice hearts and the MI hearts.

Implantation of Sarcoma Cells

S180 sarcoma was inoculated subcutaneously into the right axilla of male WT and AT1KO mice at a dose of 2×10^6 cells in 0.2 mL PBS/mouse.[15] The mice were euthanized on day 14, and the tumor was removed and weighted. The number of capillaries in the tumor was counted as described.

Statistical Analysis

Data were shown as mean±SEM. Multiple group comparison was performed by one-way ANOVA followed by the Bonferroni procedure for comparison of means. Comparison between 2 groups was analyzed by the two-tailed Student t test or two-way ANOVA. Values of $P<0.05$ were considered statistically significant.

Results

AT1 Plays a Critical Role in Neovascularization After MI

We have previously reported that an infarcted size was significantly reduced in AT1KO mice compared with WT mice.[4] We therefore examined whether AT1 was involved in angiogenesis during the remodeling process. Immunohistochemical studies using anti-PECAM antibody revealed that the number of capillaries was increased in the border zone of the infarcted hearts of WT and AT1KO mice 14 days after MI as compared with hearts of sham-operated mice (Figure 1A), and this increase was more prominent in WT mice than in AT1KO mice (Figure 1A and 1B). Immunohistochemical analysis using anti-SMA antibody showed that the number of arteriole was also increased in the border zone of the infarcted hearts of WT mice on day 14 after MI, but not of AT1KO mice (Figure 1C and 1D). These results suggest that AT1 has stimulating effects on neovascularization after MI.

There was no significant difference in the heart rate between WT mice and AT1KO mice, but SBP in AT1KO mice was lower than that in WT mice (Figure 1E), which might affect neovascularization. To examine the effect of BP on angiogenesis after MI, we administered hydralazine to WT mice. SBP in WT mice treated with hydralazine was as low as that in AT1KO mice (Figure 1E). There was no significant difference in the capillary density between WT mice with hydralazine and WT mice without the treatment (Figure 1F). These results indicate that lower BP of AT1KO did not account for decreased angiogenesis in ischemic myocardium.

AT1 Mediates Cell Infiltration After MI

Because it has been reported that inflammation is an important trigger for ischemia-induced neovascularization[16] and that the RAS plays an important role in inflammatory responses,[17] we examined infiltration of inflammatory cells in the heart after MI. The numbers of granulocytes, macrophages, and T lymphocytes were examined in the myocardium on day 4 after MI using anti-Ly6G, anti-Mac3, and anti-CD3 antibodies, respectively. Many granulocytes (Figure 2A and 2D), macrophages (Figure
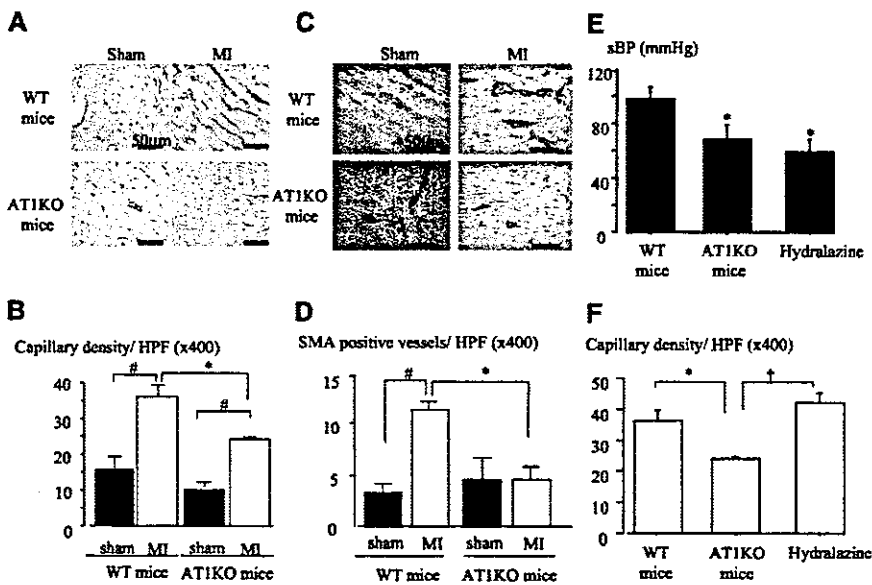
Figure 1. Neovascularization at 14 days after MI. A, The border zone of infarcted heart was stained with anti-PECAM antibody. B, Number of PECAM-positive capillaries per HPF. C, The border zone of infarcted heart was stained with anti-SMA antibody. D, Number of SMA-positive arterioles per HPF. E, Systolic blood pressure (SBP) before MI. F, Number of PECAM-positive capillaries per HPF. MI indicates myocardial infarction; WT, wild-type; AT1KO, angiotensin type1a receptor knockout; hydralazine, WT mice treated with hydralazine; HPF, high-power field. *$P<0.01$ versus WT, #$P<0.01$ versus sham, †$P<0.01$ versus AT1KO.

2B and 2E), and T lymphocytes (Figure 2C and 2F) were observed in the heart of WT and AT1KO mice after MI. The numbers of infiltrative cells such as granulocytes and macrophages were much larger in WT mice than those in AT1KO mice (Figure 2G), suggesting that AT1 is critically involved in cell infiltration in the myocardium after MI.

AT1 Induces MMPs and Activates Akt-1

Because it has been reported that MMPs are important for cell invasion into extravascular space[8] and that MMPs play a critical role in vascularization,[18] we next examined protein levels of MMP-2 and MMP-9 in the heart after MI. MMP-2 was increased on day 1 after MI in both WT mice and AT1KO mice (Figure 3A and 3B). MMP-9 was increased from day 4 in both WT mice and AT1KO mice (Figure 3A and 3C). The increases of MMP-2 and MMP-9 were more remarkable in WT mice compared with AT1KO mice (Figure 3B and 3C).

We examined another angiogenic factor, Akt-1.[19] The protein level of Akt-1 was increased in WT mice and AT1KO mice after MI (Figure 3D), and the increase was more prominent in WT mice (Figure 3E). The level of phosphorylated Akt-1 was more markedly increased after MI in WT

mice than in AT1KO mice (Figure 3D and 3F), suggesting that AngII enhances activation of Akt-1 after MI.

Activation of eNOS by AngII Induces Angiogenesis

Akt has been shown to phosphorylate and activate eNOS,[20,21] thereby promoting angiogenesis.[22,23] We therefore examined the protein level and activity of NOS in the heart after MI. There was no significant change in eNOS protein levels after MI between WT mice and AT1KO mice (Figure 4A and 4B), but the NOS activity in WT mice was higher than that in AT1KO mice (Figure 4C). Expression of vascular endothelial growth factor after MI did not differ between WT mice and AT1KO mice (data not shown).

To further elucidate the role of eNOS activity in infarcted myocardium, we administered L-NAME to WT mice to reduce NO production. Treatment with L-NAME partially but significantly reduced the capillary density in the infarcted heart of WT mice (Figure 4D). In contrast, inhibition of NO production had no effect on neovascularization after MI in AT1KO mice. These results suggest that AngII-induced eNOS activation partly regulates angiogenesis after MI.
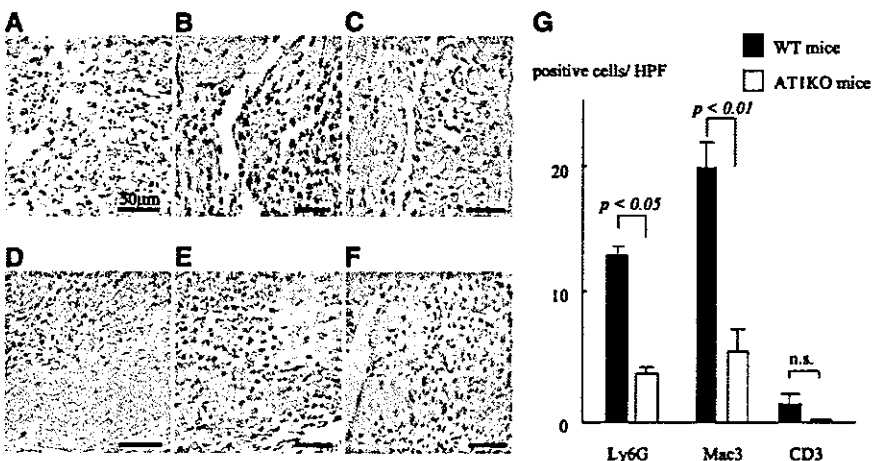

Figure 2. Cell infiltration in the myocardium at 4 days after MI. The immunohistochemical study using anti-Ly6G (granulocytes, A and D), anti-Mac3 (macrophages, B and E), and anti-CD3 (T cells, C and F) antibodies in WT mice (A, B, and C) and AT1KO mice (D, E and F). G, The number of infiltrating cells in the border zone of infarcted myocardium. Left columns show the number of Ly6G-positive cells, middle columns show the number of Mac3-positive cells, and right columns show the number of CD3-positive cells.
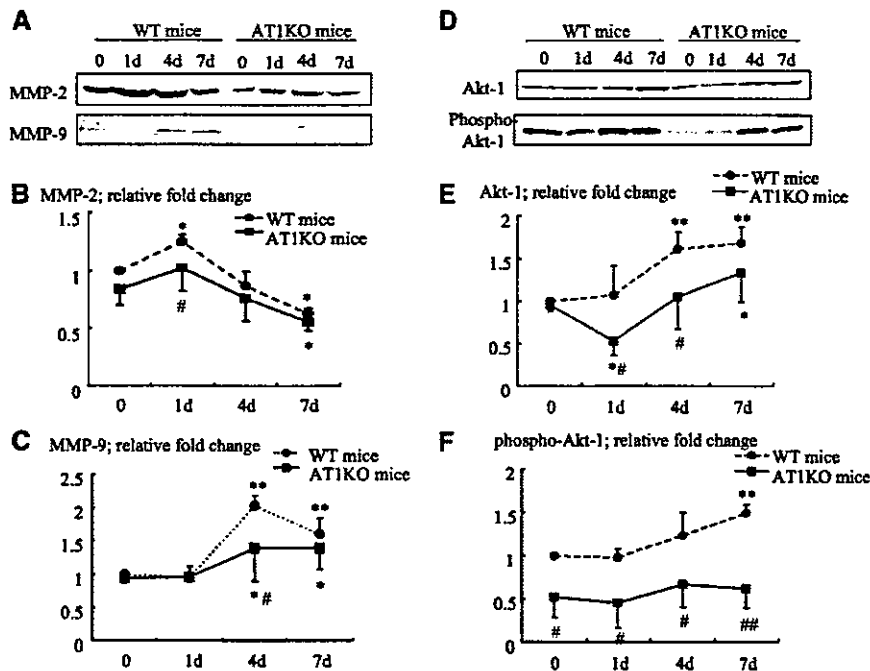
Figure 3. Protein levels of MMP-2, MMP-9, Akt-1, and phospho-Akt-1. A, Western blot analysis of MMP-2 and MMP-9 on days 0 (sham), 1, 4, and 7 after MI in WT mice and AT1KO mice. B, Relative fold change of MMP-2 protein levels. C, Relative fold change of MMP-9 protein levels. D, Western blot analysis of Akt-1 and phospho-Akt-1 on days 0 (sham), 1, 4, and 7 after MI in WT and AT1KO mice. E, Relative fold change of Akt-1 protein levels. F, Relative fold change of pospho-Akt-1 protein levels. $*P<0.05$ and $**P<0.01$ versus WT mice or AT1KO mice on day 0, $\#P<0.05$ and $\#\#P<0.01$ versus WT mice on the same day.

AT1 Is Involved in Induction of Cytokines and Chemokines in Infarcted Myocardium

Various cytokines and chemokines have been reported to play a critical role in left ventricular remodeling after MI.[24] We examined various cytokines and chemokines using ribonuclease protection assay. The expression levels of tumor necrosis factor-α, interleukin (IL)-6, transforming growth factor (TGF)-β1, TGF-β2, TGF-β3, interferon-inducible protein-10 (IP-10), monocyte chemoattractant protein-1 (MCP-1), exotoxin, RANTES, macrophage inflammatory protein (MIP)-α, MIP-1β, and MIP-2 were increased in infarcted myocardium in WT and AT1KO mice (Figure 5A and data not shown). Most of these cytokines and chemokines such as TGF-β1, TGF-β2,

TGF-β3, IP-10, MCP-1, MIP-1α, MIP-1β, and MIP-2 were more strongly upregulated in WT mice compared with AT1KO mice (Figure 5B and data not shown).

Tumor Progression Is Inhibited in AT1KO Mice

Because tumor growth depends on angiogenesis,[25] we also investigated the role of AT1 in tumor angiogenesis. The tumor size in WT mice was larger than that in AT1KO mice 14 days after implantation of sarcoma cells (Figure 6A). The much more capillaries were observed in the tumor in WT mice compared with AT1KO mice (Figure 6B and 6C). These results indicate that AngII plays an important role in angiogenesis of tumors as well as ischemic hearts.
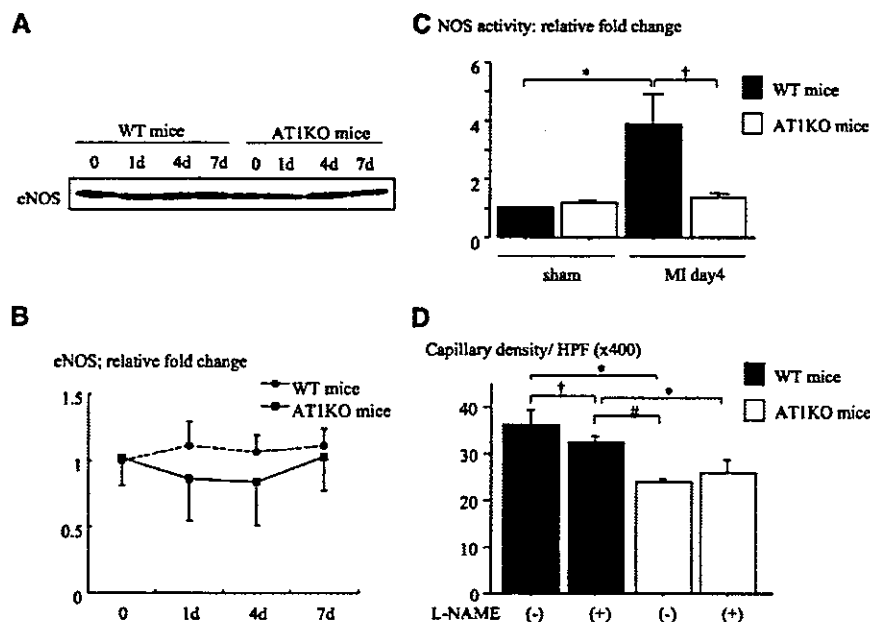

Figure 4. The effect of eNOS on angiogenesis after MI. A, Western blot analysis of eNOS on days 0 (sham), 1, 4, and 7 after MI in WT and AT1KO mice. B, Relative fold change of eNOS protein levels. C, Relative fold change of NOS activity on day 0 and day 4. $*P<0.01$ versus sham, $\#P<0.05$ versus WT mice. D, Number of PECAM-positive capillaries per HPF on day 0 and day 14 after MI with or without L-NAME treatment. $*P<0.01$, $\#P<0.01$, $\dagger P<0.05$.
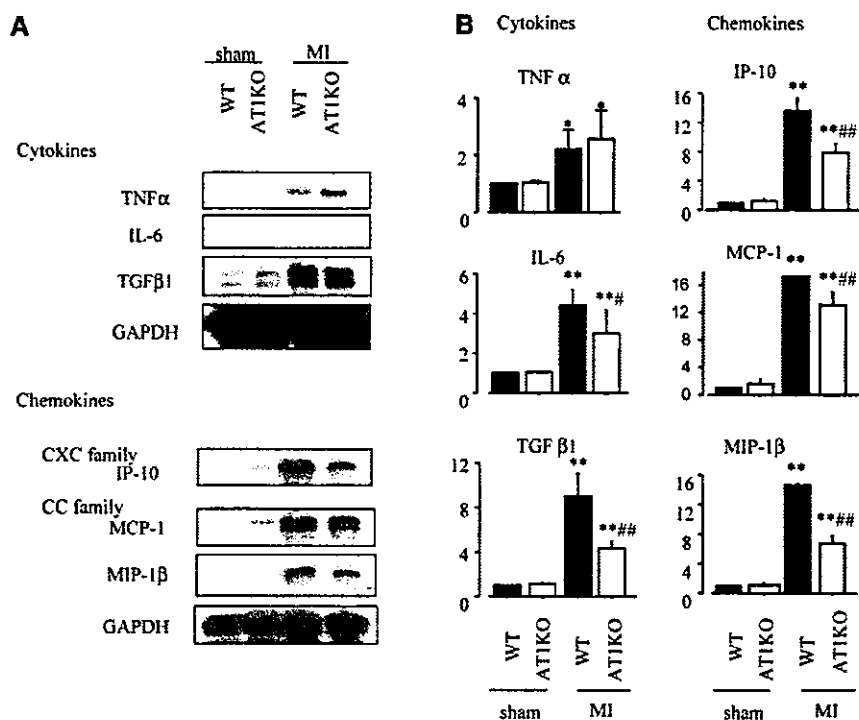
A

B   Cytokines   Chemokines

Figure 5. mRNA levels of cytokines and chemokines using RNase protection assay. A, mRNA level on day 0 (sham) and day 4 after MI in WT and AT1KO mice. B, Relative fold changes of mRNA levels. *P<0.05 and **P<0.01 versus sham, #P<0.05 and ##P<0.01 versus WT mice.

Discussion

AT1 Is Involved in Neovascularization After MI

It has been reported that an increase of neovascularization improves cardiac function and mortality,[5] and that inhibition of RAS is effective to prevent post-infarction cardiac remodeling.[1-4] It is unknown, however, whether activation of AngII/AT1 signaling induces or prevents vascularization in the infarcted heart. Some reports have demonstrated that AngII induces neovascularization in various experimental models including tumors, ischemic limb, retina, and chorioallantoic membrane.[6-8] To the contrary, there are some reports showing that inhibition of RAS induces neovascularization.[9] We thus examined in this study the role of AngII/AT1 in neovascularization during left ventricular remodeling and tumor progression using AT1KO mice. AT1KO mice exhibited less capillaries and arterioles than WT mice, suggesting that AT1 plays a pivotal role in neovascularization of the heart after MI and tumors.

AT1 Signal Plays an Important Role in Induction of MMPs and Cell Infiltration

To elucidate the molecular mechanism of how AngII induces neovascularization, we examined several molecules that have

been reported to play an important role in angiogenesis. MMP-2 and MMP-9, gelatinases that digest basement membrane and play a critical role in cell invasion,[8] have been reported to be necessary for vascularization.[18,26] It has been reported that the treatment with ACE inhibitors decreases MMP-2 at mRNA and protein levels in vitro[27] and inhibits endothelial-cell migration by blocking the activity of MMP-2 and MMP-9.[26] In this study, protein levels of MMP-2 and MMP-9 were increased after MI and the increase was attenuated in AT1KO mice compared with WT mice. Histological examination revealed that infiltration of inflammatory cells such as granulocytes and macrophages was more remarkable in WT mice than AT1KO mice. These results and observations suggest that AngII induces transendothelial migration of inflammatory cells at least in part through enhanced production of MMP-2 and MMP-9. MMPs have been also demonstrated to contribute to tissue remodeling in a number of disease states, and inhibition of MMPs prevents left ventricular remodeling after MI.[28] Mice with targeted disruption of MMP-9 have attenuated ventricular remodeling and decreased cardiac rupture after infarction.[28] Our previous report also demonstrated that left ventricular dimension was

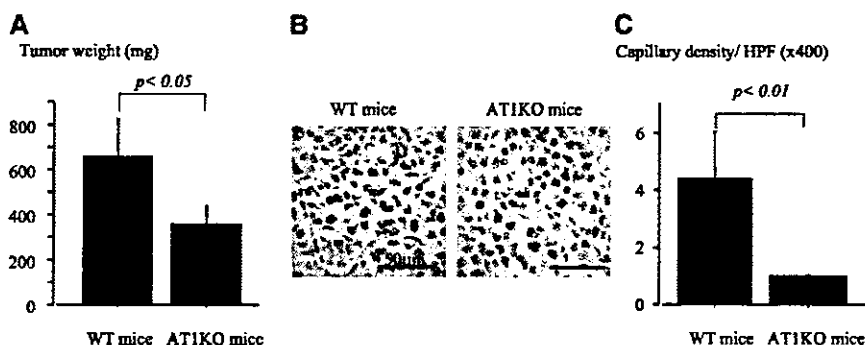A   B   C

Figure 6. Tumor size and neovascularization at 14 days after sarcoma cell transplantation. A, Tumor size at 14 days after transplantation. B, The tumor was stained with anti-PECAM antibody. C, Number of PECAM-positive capillaries/HPF.

smaller in AT1KO mice than WT mice 4 weeks after MI.[4] These results suggest that MMPs activation via the AT1 signaling pathway is involved in neovascularization as well as in post-infarcted cardiac remodeling.

Activation of Akt-1 and eNOS by AngII Induces Angiogenesis in the Infarcted Myocardium

Akt plays an important role in cell survival, cell migration and angiogenesis.[29] AngII has been shown to activate Akt,[30] Akt phosphorylates, and eNOS,[20,21] thereby promoting angiogenesis. In this study, protein levels of Akt-1 were more increased in the heart of WT mice than AT1KO mice and Akt-1 was activated only in the heart of WT mice. Although there was no significant difference in protein levels of eNOS between WT mice and AT1KO mice, eNOS activity was significantly increased in WT mice compared with AT1KO mice. Moreover, the increase of capillaries in WT mice was partially inhibited by L-NAME treatment. These results suggest that AngII-induced activation of eNOS, mediated possibly by Akt, enhances angiogenesis in ischemic myocardium.

AngII Is Involved in the Production of Various Cytokines

The inflammation in cardiovascular diseases is associated with the activation of a variety of cells including lymphocytes, monocytes/macrophage, endothelial cells, smooth muscle cells, and cardiac myocytes, which express and secrete proinflammatory cytokines and chemokines.[24] These cytokines can modulate cardiac function and cardiovascular remodeling.[24] Various cytokines were increased after MI, and the increases of TGF-β, MIP-1, IP-10, and MCP-1 were more prominent in WT mice compared with AT1KO mice. These results suggest that AngII is involved in production of various cytokines after MI, which induce post-infarcted cardiac remodeling including impaired cardiac function and increased fibrosis.

Chemokines represent a family of inflammatory cytokines that induce chemotaxis of leukocyte subsets into inflammatory tissues.[31] CC-chemokines are potent chemoattractants and activators for monocytes and lymphocytes, whereas most CXC-chemokines attract neutrophils.[32] MCP-1 recruits monocytes, which produce proteolytic enzymes, reactive oxygen species, and inflammatory cytokines.[33] Recent studies have shown that neovascularization in response to tissue ischemia depends on macrophage infiltration[34] and that local infusion of MCP-1 markedly increases collateral and peripheral conductance in hindlimb ischemia model.[35] Moreover, inflammatory cytokines such as IL-1, IL-6–related cytokines, and MCP-1 have been reported to induce myocardial dysfunction[36,37] and cardiac remodeling through promotion of cardiomyocyte hypertrophy and apoptosis as well as alteration in extracellular matrix in the myocardium.[38] The MCP-1 overexpression mice showed hypertrophied left ventricular wall, dilated left ventricular dimension, and decreased cardiac function.[39] In this study, the MCP-1 expression was suppressed and the number of macrophage infiltrated into myocardium was less in AT1KO mice after MI compared with WT mice. These results and observations suggest that reduction of MCP-1 expression and macrophage infiltration might

be related to less left ventricular remodeling despite less neovascularization in the heart of AT1KO mice.

AngII/AT1 signaling has 2 roles in left ventricular remodeling after MI. Activation of AT1 induces expression of chemokines and infiltration of inflammatory cells, which cause neovascularization possibly through enhanced expression of MMPs and activation of Akt. The enhanced neovascularization may prevent left ventricular remodeling by inhibition of cardiomyocyte apoptosis. However, AngII/AT1-induced cardiomyocyte hypertrophy, increased fibrosis, enhanced cytokines, and MMPs expressions induce left ventricular remodeling. Taken together with the previous reports,[4] inhibition of AngII/AT1 signal is important for preventing cardiac remodeling after MI, although it may suppress neovascularization.

References

1. Effect of ramipril on mortality and morbidity of survivors of acute myocardial infarction with clinical evidence of heart failure. The Acute Infarction Ramipril Efficacy (AIRE) Study Investigators. *Lancet.* 1993; 342:821–828.
2. Latini R, Maggioni AP, Flather M, Sleight P, Tognoni G. ACE inhibitor use in patients with myocardial infarction. Summary of evidence from clinical trials. *Circulation.* 1995;92:3132–3137.
3. Pfeffer MA. ACE inhibition in acute myocardial infarction. *N Engl J Med.* 1995;332:118–120.
4. Harada K, Sugaya T, Murakami K, Yazaki Y, Komuro I. Angiotensin II type 1A receptor knockout mice display less left ventricular remodeling and improved survival after myocardial infarction. *Circulation.* 1999;100: 2093–2099.
5. Kocher AA, Schuster MD, Szabolcs MJ, Takuma S, Burkhoff D, Wang J, Homma S, Edwards NM, Itescu S. Neovascularization of ischemic myocardium by human bone-marrow-derived angioblasts prevents cardiomyocyte apoptosis, reduces remodeling and improves cardiac function. *Nat Med.* 2001;7:430–436.
6. Moravski CJ, Kelly DJ, Cooper ME, Gilbert RE, Bertram JF, Shahinfar S, Skinner SL, Wilkinson-Berka JL. Retinal neovascularization is prevented by blockade of the renin-angiotensin system. *Hypertension.* 2000; 36:1099–1104.
7. Sasaki K, Murohara T, Ikeda H, Sugaya T, Shimada T, Shintani S, Imaizumi T. Evidence for the importance of angiotensin II type 1 receptor in ischemia-induced angiogenesis. *J Clin Invest.* 2002;109:603–611.
8. Vu TH, Werb Z. Matrix metalloproteinases: effectors of development and normal physiology. *Genes Dev.* 2000;14:2123–2133.
9. Fabre JE, Rivard A, Magner M, Silver M, Isner JM. Tissue inhibition of angiotensin-converting enzyme activity stimulates angiogenesis in vivo. *Circulation.* 1999;99:3043–3049.
10. Kalkman EA, van Haren P, Saxena PR, Schoemaker RG. Early captopril prevents myocardial infarction-induced hypertrophy but not angiogenesis. *Eur J Pharmacol.* 1999;369:339–348.
11. Sugaya T, Nishimatsu S, Tanimoto K, Takimoto E, Yamagishi T, Imamura K, Goto S, Imaizumi K, Hisada Y, Otsuka A, Uchida H, Sugiura M, Fukuta K, Fukamizu A, Murakami K. Angiotensin II type 1a receptor-deficient mice with hypotension and hyperreninemia. *J Biol Chem.* 1995; 270:18719–18722.
12. Toko H, Zhu W, Takimoto E, Shiojima I, Hiroi Y, Zou Y, Oka T, Akazawa H, Mizukami M, Sakamoto M, Terasaki F, Kitaura Y, Takano H, Nagai T, Nagai R, Komuro I. Csx/Nkx2-5 is required for homeostasis and survival of cardiac myocytes in the adult heart. *J Biol Chem.* 2002; 277:24735–24743.

13. Harada K, Komuro I, Shiojima I, Hayashi D, Kudoh S, Mizuno T, Kijima K, Matsubara H, Sugaya T, Murakami K, Yazaki Y. Pressure overload induces cardiac hypertrophy in angiotensin II type 1A receptor knockout mice. *Circulation.* 1998;97:1952–1959.

14. Toko H, Oka T, Zou Y, Sakamoto M, Mizukami M, Sano M, Yamamoto R, Sugaya T, Komuro I. Angiotensin II type 1a receptor mediates doxorubicin-induced cardiomyopathy. *Hypertens Res.* 2002;25:597–603.

15. Wang G, Dong Z, Xu G, Yang Z, Shou C, Wang N, Liu T. The effect of antibody against vascular endothelial growth factor on tumor growth and metastasis. *J Cancer Res Clin Oncol.* 1998;124:615–620.

16. Salven P, Hattori K, Heissig B, Rafii S. Interleukin-1alpha promotes angiogenesis in vivo via VEGFR-2 pathway by inducing inflammatory cell VEGF synthesis and secretion. *FASEB J.* 2002;16:1471–1473.

17. Nicoletti A, Michel JB. Cardiac fibrosis and inflammation: interaction with hemodynamic and hormonal factors. *Cardiovasc Res.* 1999;41: 532–543.

18. Hiraoka N, Allen E, Apel IJ, Gyetko MR, Weiss SJ. Matrix metalloproteinases regulate neovascularization by acting as pericellular fibrinolysins. *Cell.* 1998;95:365–377.

19. Jiang BH, Zheng JZ, Aoki M, Vogt PK. Phosphatidylinositol 3-kinase signaling mediates angiogenesis and expression of vascular endothelial growth factor in endothelial cells. *Proc Natl Acad Sci U S A.* 2000;97: 1749–1753.

20. Dimmeler S, Fleming I, Fisslthaler B, Hermann C, Busse R, Zeiher AM. Activation of nitric oxide synthase in endothelial cells by Akt-dependent phosphorylation. *Nature.* 1999;399:601–605.

21. Fulton D, Gratton JP, McCabe TJ, Fontana J, Fujio Y, Walsh K, Franke TF, Papapetropoulos A, Sessa WC. Regulation of endothelium-derived nitric oxide production by the protein kinase Akt. *Nature.* 1999;399: 597–601.

22. Matsunaga T, Warltier DC, Weihrauch DW, Moniz M, Tessmer J, Chilian WM. Ischemia-induced coronary collateral growth is dependent on vascular endothelial growth factor and nitric oxide. *Circulation.* 2000; 102:3098–3103.

23. Murohara T, Asahara T, Silver M, Bauters C, Masuda H, Kalka C, Kearney M, Chen D, Symes JF, Fishman MC, Huang PL, Isner JM. Nitric oxide synthase modulates angiogenesis in response to tissue ischemia. *J Clin Invest.* 1998;101:2567–2578.

24. Frangogiannis NG, Smith CW, Entman ML. The inflammatory response in myocardial infarction. *Cardiovasc Res.* 2002;53:31–47.

25. Folkman J. Angiogenesis in cancer, vascular, rheumatoid and other disease. *Nat Med.* 1995;1:27–31.

26. Volpert OV, Ward WF, Lingen MW, Chesler L, Solt DB, Johnson MD, Molteni A, Polverini PJ, Bouck NP. Captopril inhibits angiogenesis and slows the growth of experimental tumors in rats. *J Clin Invest.* 1996;98: 671–679.

27. Prontera C, Mariani B, Rossi C, Poggi A, Rotilio D. Inhibition of gelatinase A (MMP-2) by batimastat and captopril reduces tumor growth and lung metastases in mice bearing Lewis lung carcinoma. *Int J Cancer.* 1999;81:761–766.

28. Heymans S, Luttun A, Nuyens D, Theilmeier G, Creemers E, Moons L, Dyspersin GD, Cleutjens JP, Shipley M, Angellilo A, Levi M, Nube O, Baker A, Keshet E, Lupu F, Herbert JM, Smits JF, Shapiro SD, Baes M, Borgers M, Collen D, Daemen MJ, Carmeliet P. Inhibition of plasminogen activators or matrix metalloproteinases prevents cardiac rupture but impairs therapeutic angiogenesis and causes cardiac failure. *Nat Med.* 1999;5:1135–1142.

29. Shiojima I, Walsh K. Role of Akt signaling in vascular homeostasis and angiogenesis. *Circ Res.* 2002;90:1243–1250.

30. Ushio-Fukai M, Alexander RW, Akers M, Yin Q, Fujio Y, Walsh K, Griendling KK. Reactive oxygen species mediate the activation of Akt/ protein kinase B by angiotensin II in vascular smooth muscle cells. *J Biol Chem.* 1999;274:22699–22704.

31. Taub DD, Oppenheim JJ. Chemokines, inflammation and the immune system. *Ther Immunol.* 1994;1:229–246.

32. Baggiolini M, Dewald B, Moser B. Interleukin-8 and related chemotactic cytokines–CXC and CC chemokines. *Adv Immunol.* 1994;55:97–179.

33. Ruiz-Ortega M, Bustos C, Hernandez-Presa MA, Lorenzo O, Plaza JJ, Egido J. Angiotensin II participates in mononuclear cell recruitment in experimental immune complex nephritis through nuclear factor-kappa B activation and monocyte chemoattractant protein-1 synthesis. *J Immunol.* 1998;161:430–439.

34. Polverini PJ, Cotran PS, Gimbrone MA, Jr., Unanue ER. Activated macrophages induce vascular proliferation. *Nature.* 1977;269:804–806.

35. Risau W. Mechanisms of angiogenesis. *Nature.* 1997;386:671–674.

36. Finkel MS, Oddis CV, Jacob TD, Watkins SC, Hattler BG, Simmons RL. Negative inotropic effects of cytokines on the heart mediated by nitric oxide. *Science.* 1992;257:387–389.

37. Yokoyama T, Vaca L, Rossen RD, Durante W, Hazarika P, Mann DL. Cellular basis for the negative inotropic effects of tumor necrosis factor-alpha in the adult mammalian heart. *J Clin Invest.* 1993;92: 2303–2312.

38. Bozkurt B, Kribbs SB, Clubb FJ, Jr., Michael LH, Didenko VV, Hornsby PJ, Seta Y, Oral H, Spinale FG, Mann DL. Pathophysiologically relevant concentrations of tumor necrosis factor-alpha promote progressive left ventricular dysfunction and remodeling in rats. *Circulation.* 1998;97: 1382–1391.

39. Kolattukudy PE, Quach T, Bergese S, Breckenridge S, Hensley J, Altschuld R, Gordillo G, Klenotic S, Orosz C, Parker-Thornburg J. Myocarditis induced by targeted expression of the MCP-1 gene in murine cardiac muscle. *Am J Pathol.* 1998;152:101–111.

Diabetologia

Oxidative stress induces insulin resistance by activating the nuclear factor-κB pathway and disrupting normal subcellular distribution of phosphatidylinositol 3-kinase

T. Ogihara[1, 2] · T. Asano[1] · H. Katagiri[2] · H. Sakoda[3] · M. Anai[3] · N. Shojima[1] · H. Ono[3] · M. Fujishiro[1] · A. Kushiyama[1] · Y. Fukushima[1] · M. Kikuchi[3] · N. Noguchi[4] · H. Aburatani[4] · Y. Gotoh[5] · I. Komuro[6] · T. Fujita[1]

[1] Department of Internal Medicine, Graduate School of Medicine, University of Tokyo, Tokyo, Japan
[2] Division of Advanced Therapeutics for Metabolic Diseases, Center for Translational and Advanced Animal Research on Human Diseases, Tohoku University Graduate School of Medicine, Sendai, Japan
[3] The Institute for Adult Diseases, Asahi Life Foundation, Tokyo, Japan
[4] Research Center for Advanced Science and Technology, University of Tokyo, Tokyo, Japan
[5] Department of Molecular Biology, Institute of Molecular and Cellular Biosciences, University of Tokyo, Tokyo, Japan
[6] Department of Cardiovascular Science and Medicine, Chiba University Graduate School of Medicine, Chiba, Japan

Abstract

Aims/hypothesis. Oxidative stress is associated with diabetes, hypertension and atherosclerosis. Insulin resistance is implicated in the development of these disorders. We tested the hypothesis that oxidative stress induces insulin resistance in rats, and endeavoured to identify mechanisms linking the two.

Methods. Buthionine sulfoximine (BSO), an inhibitor of glutathione synthase, was administered to Sprague-Dawley rats and 3T3-L1 adipocytes. Glucose metabolism and insulin signalling both in vivo and in 3T3-L1 adipocytes were examined. In 3T3-L1 adipocytes, the effects of overexpression of a dominant negative mutant of inhibitory κB (IκB), one role of which is to block oxidative-stress-induced nuclear factor (NF)-κB activation, were investigated.

Results. In rats given BSO for 2 weeks, the plasma lipid hydroperoxide level doubled, indicating increased oxidative stress. A hyperinsulinaemic-euglycaemic clamp study and a glucose transport assay using isolated muscle and adipocytes revealed insulin resistance in BSO-treated rats. BSO treatment also impaired insulin-induced glucose uptake and GLUT4 translocation in 3T3-L1 adipocytes. In BSO-treated rat muscle, adipose tissue and 3T3-L1 adipocytes, insulin-induced IRS-1 phosphorylation in the low-density microsome (LDM) fraction was specifically decreased, while that in whole cell lysates was not altered, and subsequent translocation of phosphatidylinositol (PI) 3-kinase from the cytosol and the LDM fraction was disrupted. BSO-induced impairments of insulin action and insulin signalling were reversed by overexpressing the dominant negative mutant of IκB, thereby suppressing NF-κB activation.

Conclusions/interpretation. Oxidative stress induces insulin resistance by impairing IRS-1 phosphorylation and PI 3-kinase activation in the LDM fraction, and NF-κB activation is likely to be involved in this process.

Keywords Buthionine sulfoximine · Glutathione · Hyperinsulinaemic-euglycaemic clamp · Inhibitory κB · Insulin resistance · IRS · Nuclear factor-κB · Oxidative stress · Phosphatidylinositol 3-kinase

T. Asano (✉)
Department of Internal Medicine, Graduate School of Medicine, University of Tokyo, Tokyo 113-8655, Japan
E-mail: asano-tky@umin.ac.jp
Tel.: +81-3-38153411 ext. 33133, Fax: +81-3-58031874

Present address:
T. Asano
Department of Physiological Chemistry and Metabolism, Graduate School of Medicine, University of Tokyo, Tokyo 113-8655, Japan

Introduction

Oxidative stress represents an imbalance between production of reactive oxygen species and the antioxidant defence system [1]. Oxidative stress is widely recognised as being associated with various disorders including diabetes, hypertension and atherosclerosis. In-

sulin resistance is a common feature of these disorders [2, 3]. Indeed, in diabetic people and in animal models of diabetes, the plasma free radical concentration is increased [4, 5] and antioxidant defences are diminished [6, 7]. It has also been suggested that antioxidant agents such as vitamin C [8] and E [9] improve insulin action in diabetic subjects.

Angiotensin II reportedly induces free radical production and increases plasma oxidative stress [10]. In our previous study, we showed continuous infusion of angiotensin II to induce insulin resistance with increased oxidative stress in rats, while the spin trap agent tempol [11], which works as a superoxide dismutase mimetic, decreases oxidative stress and improves insulin resistance in these rats [12]. A similar coexistence of oxidative stress and insulin resistance, as well as recovery with tempol administration was observed in adrenomedullin-deficient mice [13]. These previous reports strongly suggest a close relationship between oxidative stress and insulin resistance. Thus, we attempted to elucidate the molecular mechanisms underlying insulin resistance and oxidative stress.

In this study, to increase oxidative stress in vivo, we utilised a selective inhibitor of γ-glutamylcysteine synthetase, i.e. an inhibitor of glutathione synthase, buthionine sulfoximine (BSO). Glutathione is one of the major components of the antioxidant defence system, such that BSO administration increases oxidative stress by reducing the tissue glutathione level [14]. Although BSO does not have toxic effects in animals [14], BSO-treated rats were previously shown to exhibit glucose intolerance [15] and hypertension [16]. In the current study, we examined the effect of BSO treatment on insulin resistance in rats and 3T3-L1 adipocytes. We investigated the molecular mechanisms underlying BSO-induced insulin resistance, focusing on the subcellular distribution of phosphatidylinositol (PI) 3-kinase. Finally, we examined the involvement of the nuclear factor (NF)-κB pathway in BSO-induced insulin resistance and insulin signalling impairment.

Materials and methods

Materials. Affinity-purified antibodies against IRS-1 and GLUT4 were prepared as previously described [17]. Antibodies against phosphotyrosine, the p85 subunit of PI 3-kinase, and inhibitory κB (IκB) were purchased from Upstate Biotechnology (Milton Keynes, UK). TNF-α and buthionine-[S, R]-sulfoximine (BSO) were purchased from Sigma-Aldrich (St. Louis, Mo., USA).

Animals. Seven-week-old male Sprague-Dawley rats (Tokyo Experimental Animals, Tokyo, Japan) were fed a standard rodent diet with or without water containing 30 mmol/l BSO for 14 days [16]. The animal care was in accordance with the policies of the University of Tokyo, and the "Principles of laboratory animal care" (NIH publication no. 85-23, revised 1985) were followed.

Measurements. Cholesteryl ester hydroperoxides were analysed by HPLC, with 234 nm UV detection and post-column chemiluminescence detection on an LC-8 column (Supelco, 4×250 mm, 5-μm particles; Sigma-Aldrich) and methanol/tert-butyl alcohol (95/5 vol) as the eluent, as reported previously but with slight modification [18]. In brief, plasma was extracted with 10 volumes of methanol and 50 volumes of hexane. The hexane phase was removed, dried under N_2 gas and redissolved in an eluent for HPLC injection. Liver glutathione content was measured spectrophotometrically using a glutathione reductase recycling assay, as described previously [19].

Hyperinsulinaemic-euglycaemic clamp study. Rats fasted overnight were anaesthetised by intraperitoneal injection of pentobarbital sodium (60 mg/kg body weight) and the left jugular and femoral veins were catheterised for blood sampling and infusion respectively. Hyperinsulinaemic-euglycaemic clamp analysis was performed as described previously [17]. The glucose utilisation rate, hepatic glucose production and an estimate of muscle glucose uptake during the clamp (defined as the glucose metabolic index) were calculated as previously described [20].

Glucose uptake into isolated soleus muscle. Rats fasted overnight were anaesthetised and soleus muscles were dissected out and rapidly cut into 20–40 mg strips. The rats were then killed by intracardiac injection of pentobarbital. Isolated soleus muscle was incubated for 20 min with or without 1.44×10^{-8} mol/l human insulin (this concentration is equivalent to 2 mU/ml), as described previously [17]. 2-Deoxy glucose uptake into the isolated soleus muscle strips was measured using 2-deoxy-D-[³H]glucose and [¹⁴C]manitol as described previously [21].

Preparation of rat adipocytes and measurement of glucose uptake. Isolated rat adipocytes were prepared from epididymal adipose tissue harvested from fasted rats using the collagenase method [22], and 2-deoxy glucose uptake was then assayed as previously described [23].

Adenovirus-mediated gene transfer to 3T3-L1 adipocytes. 3T3-L1 fibroblasts were maintained in DMEM supplemented with 10% donor calf serum and differentiated into adipocytes as previously described [24]. The dominant negative mutant of IκB-α, in which serine residues 32 and 36 were substituted with alanine, was kindly provided by Dr R. Gaynor (University of Texas Southwestern Medical Center at Dallas, Tex., USA). To obtain recombinant adenovirus, pAdeno-X was ligated with cDNA encoding *Escherichia coli* lacZ and dominant negative IκB according to the manufacturer's instructions for the Adeno-X Expression System (Clontech, Palo Alto, Calif., USA). Infection of 3T3-L1 adipocytes with the adenovirus was carried out as described previously [25]. Recombinant adenoviruses were applied at a multiplicity of infection of approximately 200–300 pfu/cell and 3T3-L1 adipocytes infected with lacZ virus were used as a control.

Gel mobility shift assay. Nuclear protein extracts from 3T3-L1 adipocytes were prepared using NE-PER nuclear and cytoplasmic extraction reagents (Pierce Biotechnology, Rockford, Ill., USA) according to the manufacturer's instructions and used for gel mobility shift assay (GMSA). Briefly, 3T3-L1 adipocytes were homogenised in 1 ml of PBS and centrifuged for 10 min at 500 × g at 4 °C. After removing the supernatant, the pellet was resuspended in 500 μl of Cytoplasmic Extraction Reagent I buffer containing protease inhibitors (1 600 mol/l benzamidine, 0.3 mmol/l aprotinin, 4.2 mol/l leupeptin, 0.2 mol/l phenylmethylsulfonyl fluoride), and was incubated

on ice for 10 min. Then, 27.5 µl of Cytoplasmic Extraction Reagent II buffer were added to the sample, which was vortexed and centrifuged at 16 000 × g for 5 min. The resultant pellet was resuspended in 250 µl of NER buffer, vortexed every 10 minutes for 40 min and then centrifuged at 16 000 × g for 10 min. The supernatant containing nuclear proteins was stored at −80 °C. For the GMSA, 10 µg of nuclear proteins were incubated in binding buffer with 3.5 pmol of double-stranded DNA oligonucleotide containing an NF-κB consensus-binding sequence labelled with [^{32}P]-ATP using T4 polynucleotide kinase for 30 min at 37 °C. For supershift analyses, monoclonal antibody against NF-κB p65 was separately pre-incubated with nuclear extracts at 4 °C for 20 min in a total volume of 16 µl of binding buffer, followed by incubation with 8 µl of ^{32}P-labelled oligonucleotide probe with and without cold oligonucleotide probe at 4 °C for 20 min using a Nushift Kit (Geneka Biotechnology, Carlsbad, Calif., USA). Protein-DNA complexes were separated from the unbound DNA probe by electrophoresis through 5% polyacrylamide gels containing 1× Tris-glycine-EDTA buffer. The gel was dried and exposed to BAS2000 (Fujifilm, Tokyo, Japan).

Glucose uptake into 3T3-L1 adipocytes. 3T3-L1 adipocytes plated in 24-well culture dishes were serum starved for 3 h in DMEM containing 0.2% bovine serum albumin, after which they were incubated in Krebs–Ringer phosphate buffer for an additional 45 min, prior to incubation with or without 10^{-6} or 10^{-7} mol/l insulin for 15 min. The assay was initiated by adding 2-deoxy-D-[^{3}H]glucose (1.85 × 10^7 Bq/sample, 0.1 mmol) and was terminated 4 min later by washing the cells once with ice-cold Krebs–Ringer phosphate buffer containing 0.3 mmol/l phloretin and then twice with ice-cold Krebs–Ringer phosphate buffer. The cells were then solubilised in 0.1% SDS, and the incorporated radioactivity was determined by scintillation counting [26].

Subcellular fractionation. 3T3-L1 adipocytes were serum starved for 3 h and incubated with or without 10^{-6} mol/l insulin for 15 min. Cells were fractionated as described previously [27]. Briefly, 3T3-L1 adipocytes were resuspended in HES buffer (255 mmol/l sucrose, 20 mmol/l HEPES [pH 7.4], 1 mmol/l EDTA), homogenised and subjected to differential centrifugation. The supernatants from the following spins were serially removed and pelleted in a Ti70 rotor as follows: 19 000 × g (20 min), 41 000 × g (20 min) and 180 000 × g (75 min). The first 19 000 × g pellet was resuspended, loaded onto a sucrose cushion (1.12 mol/l sucrose, 20 mmol/l HEPES [pH 7.4], 1 mmol/l EDTA) and isolated from the interface yielding the plasma membrane fraction as the pellet of a 41 000 × g spin (20 min). The last 180 000 × g pellet corresponded to the low-density microsome (LDM) fraction. Subcellular fractionation and measurement of GLUT4 translocation in isolated skeletal muscle and adipocytes from rats were described previously [12]. After resuspension of the pellets in solubilisation buffer, 20 µg of each fraction were loaded for western blotting. Proteins in the plasma membrane and LDM fractions were separated by SDS-PAGE, transferred to a polyvinylidene fluoride membrane, immunoblotted with anti-GLUT4, anti-IRS-1 or anti-p85 antibodies, and reacted with enhanced chemiluminescence reagent (Amersham Biosciences, Uppsala, Sweden) or subject to immunoprecipitation and PI 3-kinase assay of the immunoprecipitates as previously described [17].

Immunoprecipitation and immunoblotting. In rat experiments, rats fasted overnight were anaesthetised, and within 10–15 min the abdominal cavity was opened, the portal vein exposed, and

16 ml/kg body weight of normal saline (0.9% NaCl), with or without 10^{-5} mol/l human insulin, were injected. After 60 s, hindlimb muscles were removed and immediately homogenised as described previously [28]. In 3T3-L1 experiments, 3T3-L1 adipocytes were serum-starved for 18 h, pre-incubated with or without 80 µmol/l BSO for 18 h, then stimulated with or without 10^{-6} mol/l insulin for 15 min. The cells were then washed and lysed with lysis buffer as described previously [29]. After centrifugation, the resultant supernatants were used for immunoprecipitation or immunoblotting as described previously [28]. Proteins were visualised with enhanced chemiluminescence and band intensities were quantified with a Molecular Imager GS-525 using Imaging Screen-CH (Bio-Rad Laboratories, Hercules, Calif., USA). In some experiments, 3T3-L1 cells were incubated with 5.8 pmol/l (equivalent to 10 ng/dl) TNF-α or 80 µmol/l BSO for 18 h, lysed and immunoblotted with anti-IκB antibody.

Phosphatidylinositol 3-kinase activity. After preparing tissue samples as above, IRS-1 was immunoprecipitated, and PI 3-kinase activity in the immunoprecipitates was assayed as previously described [17].

Statistical analysis. Data are expressed as means ± SE. Comparisons between the two groups were made using unpaired *t* tests. We considered *p* values of less than 0.05 to be statistically significant.

Results

Characterisation of rats studied. Although food intakes were similar in the two groups, the BSO-treated rats had lower body weights than control rats (Table 1). Individual water consumptions did not differ between the two. Systolic and diastolic blood pressures were similar in the two groups of rats. Fasting blood glucose and plasma insulin levels in BSO rats were also similar to those of control rats. Although fasting insulin levels were not elevated in BSO-treated rats as compared with those of controls, we found that

Table 1. Characterisation of BSO-treated rats

	Control	BSO
Body weight (g)	320.0±8.7	284±4.1*
Food intake (g/day)	20.2±2.4	21.2±2.3
Water intake (ml/day)	38.2±1.8	36.8±3.2
Systolic BP (mm Hg)	113.5±4.4	120.7±3.9
Diastolic BP (mm Hg)	83.4±4.4	87.8±1.4
Fasting blood glucose (mmol/l)	6.12±0.32	6.32±0.24
Randomly fed blood glucose (mmol/l)	8.37±0.24	8.44±0.17
Fasting plasma insulin (pmol/l)	109±16	112±3
Randomly fed plasma insulin (pmol/l)	188±17	367±3*
Glutathione content of liver (µmol/g tissue)	3.2±0.3	1.1±0.4*
Plasma cholesteryl ester hydroperoxide (mmol/l)	1.38±0.3	2.72±0.3*

Data are means ± SE; rats in each group, *n*=6; * *p*<0.05 compared with controls

a   b   c   d

Glucose infusion rate (mg·kg⁻¹·min⁻¹)
Glucose utilisation rate (mg·kg⁻¹·min⁻¹)
Hepatic glucose production (mg·kg⁻¹·min⁻¹)
Glucose uptake into muscle during the clamp (mmol·100g⁻¹·min⁻¹)

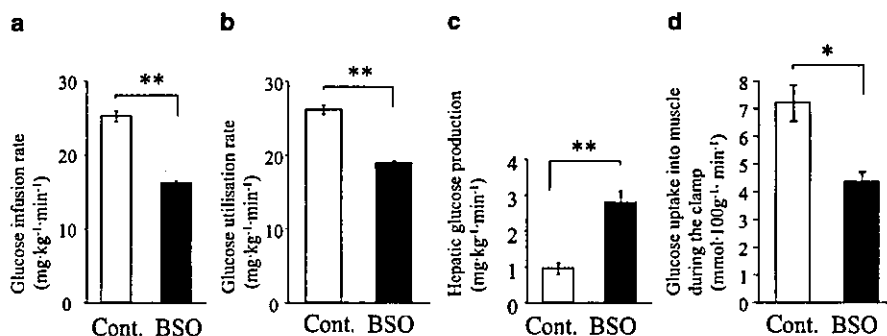Cont. BSO   Cont. BSO   Cont. BSO   Cont. BSO

Fig. 1. A hyperinsulinaemic-euglycaemic clamp study. Rats were anaesthetised by intraperitoneal injection of pentobarbital sodium and the left jugular and femoral veins were catheterised for blood sampling and infusion respectively. Hyperinsulinaemic-euglycaemic clamp analysis was performed as described previously [17]. The glucose infusion rate (a), glucose utilisation rate (b), hepatic glucose production (c) and muscle glucose uptake during the clamp (defined as the glucose metabolic index; d) were estimated from hyperinsulinaemic-euglycaemic clamp data. *$p<0.05$, **$p<0.01$ compared with the control. Bars represent the means ± SE of results from four to five rats. Cont. indicates control Sprague-Dawley rats. BSO indicates rats fed a standard rodent diet with water containing 30 mmol/l BSO for 12 days

among well-fed animals, insulin levels in BSO-treated rats were significantly higher than those in controls. To determine the effect of BSO as a glutathione synthase inhibitor, hepatic glutathione content was measured, because glutathione is most abundant in the liver. The glutathione level was significantly lower, by 34%, in the livers of BSO-treated rats than in those of controls. The cholesteryl ester hydroperoxide level in BSO-treated rat plasma was double that in control rats, suggesting that oxidative stress is increased in BSO-treated rats.

Hyperinsulinaemic-euglycaemic clamp study. Whole-body insulin sensitivity was evaluated using a hyperinsulinaemic-euglycaemic clamp technique. Compared with controls, the glucose infusion rate was decreased by 36.2% and the glucose utilisation rate by 27.6% during submaximal insulin infusion in BSO-treated rats (Figs. 1a, b). In addition, hepatic glucose production was increased by 29.3% in BSO-treated rats, suggesting impairment of the ability of insulin to suppress hepatic glucose production (Fig. 1c). Glucose uptake into skeletal muscle during the clamp was decreased by 39.4% in BSO-treated rats (Fig. 1d). These results suggest that BSO treatment induces insulin resistance both systemically and in skeletal muscle and liver.

Insulin-induced glucose uptake and GLUT4 translocation in BSO-treated rat skeletal muscle and adipocytes. In BSO-treated rats, insulin-induced glucose uptakes

into isolated soleus muscle and adipocytes were reduced by 21.4% and 47.8% respectively as compared with the control levels (Figs. 2a, c). Subsequent western blot analysis showed the GLUT4 contents of skeletal muscle and adipocytes to be similar in the two groups (Figs. 2b, d, upper panels), indicating that the impairment of insulin-induced glucose uptake in these tissues from BSO-treated rats was not due to reduced expression of GLUT4 proteins. However, insulin-induced GLUT4 translocation, as assessed by the appearance of GLUT4 in the plasma membrane fraction of skeletal muscle and adipose tissue, was decreased in BSO-treated rats (Figs. 2b, d, lower panels). Microscopic analysis revealed adipocytes from BSO-treated rats to be small, which is consistent with the low body weights of these rats (Fig. 2e), suggesting that insulin resistance in BSO-treated rats is not attributable to adipocyte enlargement.

Impairment of insulin signalling in BSO-treated rat skeletal muscle and adipocytes. Next, we investigated insulin-induced tyrosine phosphorylation of IRS-1, association of PI 3-kinase with IRS-1, and PI 3-kinase activation in skeletal muscle and adipose tissue in vivo by injecting insulin through the portal vein of anaesthetised rats. Protein amount and insulin-induced tyrosine phosphorylation of IRS-1 in skeletal muscle (whole tissue lysates) from BSO-treated rats were similar to those in controls (Fig. 3a, upper panels). Because the insulin signalling in the LDM fraction has been implicated in several insulin actions including insulin-induced glucose uptake [30, 31], we carried out subcellular fractionation studies of skeletal muscles from these rats. Subcellular fractionation data showed insulin-induced tyrosine phosphorylation of IRS-1 in the LDM fraction to be significantly decreased in BSO-treated rats as compared with controls, although the IRS-1 protein amount in this fraction was unchanged (Fig. 3a, upper panels). In the cytosol, the amount of IRS-1 and insulin-induced phosphorylation were similar in BSO-treated and control rat muscles (Fig. 3a, upper panels). Next, we investigated the amount of the p85 subunit for PI 3-kinase protein in whole tissue lysates, the LDM fraction and the cytosol (Fig. 3a, middle panels). The amounts of p85 protein were similar in whole tissue
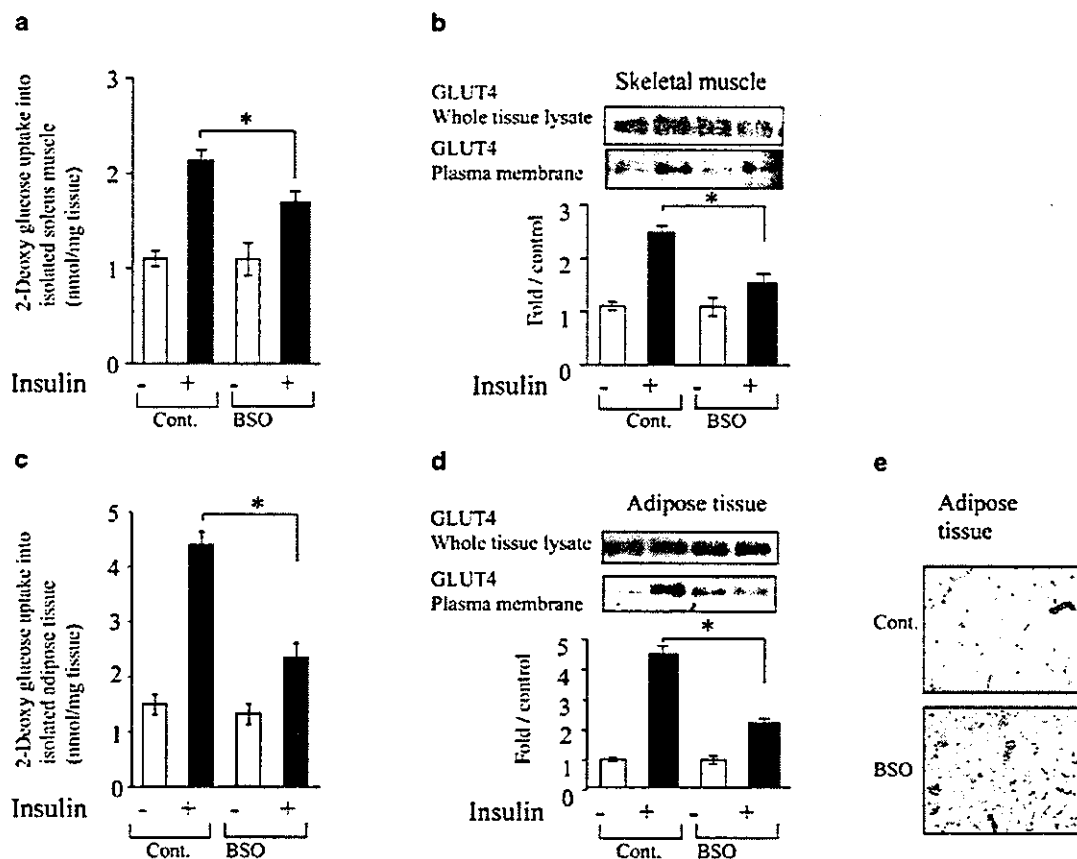
a

2-Deoxy glucose uptake into isolated soleus muscle (nmol/mg tissue)

Insulin

Cont.   BSO

b

GLUT4 Whole tissue lysate
GLUT4 Plasma membrane

Skeletal muscle

Fold / control

Insulin

Cont.   BSO

c

2-Deoxy glucose uptake into isolated adipose tissue (nmol/mg tissue)

Insulin

Cont.   BSO

d

GLUT4 Whole tissue lysate
GLUT4 Plasma membrane

Adipose tissue

Fold / control

Insulin

Cont.   BSO

e

Adipose tissue

Cont.

BSO

Fig. 2. Insulin resistance in isolated skeletal muscle and adipose tissue in BSO-treated rats. a. 2-Deoxy-glucose uptakes into isolated soleus muscle and adipose tissue (c). Isolated rat soleus muscle was incubated for 20 min with or without 1.44×10⁻⁸ mol/l human insulin (this concentration is equivalent to 2 mU/ml) as described previously [17]. 2-Deoxy-D-[1-³H]glucose uptake into the isolated soleus muscle strips was measured as described previously [21]. Isolated rat adipocytes were prepared from epididymal adipose tissue harvested from fasted rats using the collagenase method [22], and 2-deoxy glucose uptake was then assayed as previously described [23]. b, d. GLUT4 protein amount in whole tissue lysates (upper panels), the plasma membrane fraction (lower panels) of skeletal muscle (b) and adipose tissue (d) under basal or insulin-stimulated conditions. Subcellular fractionation and measurement of GLUT4 translocation of isolated skeletal muscle and adipocytes from rats were described previously [12]. Whole tissue lysates and plasma membrane fractions were subjected to SDS-PAGE followed by immunoblotting with anti-GLUT4 antibody. The data are representative of three independent experiments. Bars depict means ± SE of the results from four to six samples. * p<0.05 compared with the control under the insulin-stimulated conditions. d. Haematoxylin and eosin stained adipose tissues from control and BSO-treated rats are shown. Cont. indicates control Sprague-Dawley rats. BSO indicates rats fed a standard rodent diet with water containing 30 mmol/l BSO for 12 days

lysates before and after insulin stimulation. However, insulin stimulation induced a p85 increase in the LDM fraction and a decrease in the cytosol, suggesting that insulin stimulates p85 translocation from the cytosol to the LDM fraction. This insulin-induced translocation of p85 was disrupted in BSO-treated rats. Insulin-induced increases in IRS-1-associated p85 protein and PI 3-kinase activity did not differ significantly between whole tissue lysates and the cytosol in either BSO-treated or control rat muscle (Fig. 3a, lower panels). However, both were significantly decreased in the LDM fraction of BSO-treated rats as compared with the controls. We obtained essentially the same results in the adipose tissue of these rats (Fig. 3b). In addition, we confirmed that insulin-induced tyrosine phosphorylation of the insulin receptor and IRS-2, as well as Ser-473 phosphorylation of Akt, in the whole tissue lysates of skeletal muscle and adipose tissue does not differ between BSO-treated and control rats (data not shown). Thus, early insulin-signalling steps were shown to be impaired specifically in the LDM fraction, but not in whole tissue lysates of skeletal muscle and adipose tissue from BSO-treated rats.

Insulin action and insulin signalling in BSO-treated 3T3-L1 adipocytes. To further investigate the impaired step in BSO-induced insulin resistance, 3T3-L1
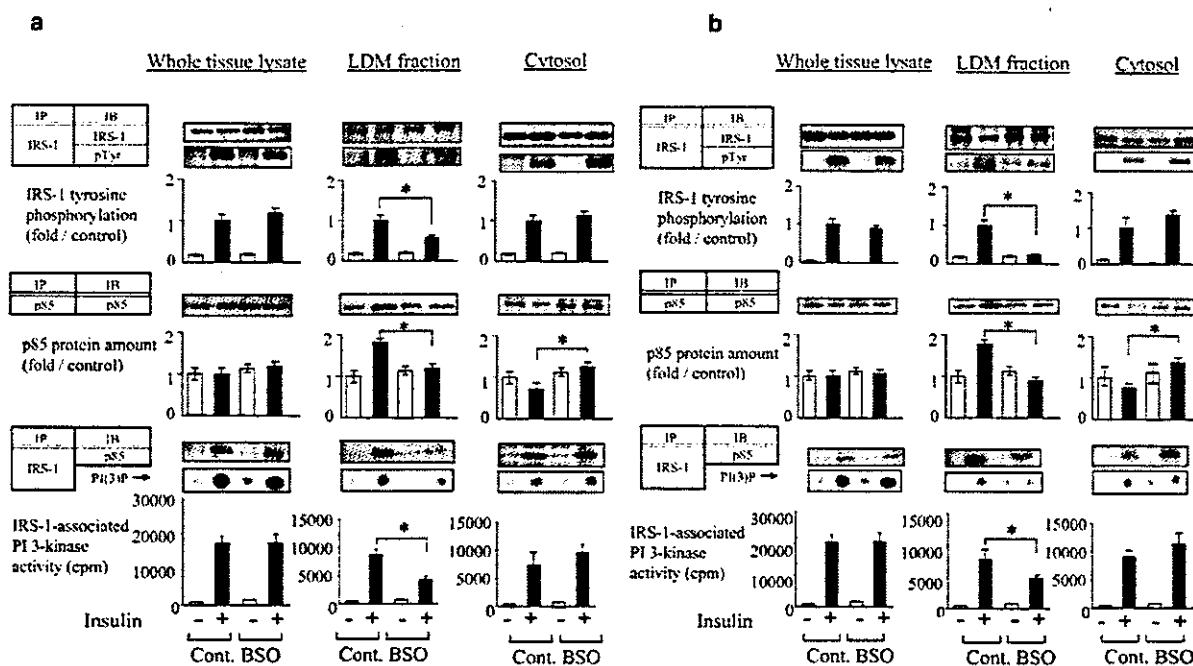
a

b

Fig. 3. Insulin signalling in skeletal muscle (a) and adipose tissue (b) from BSO-treated rats. Rats were anaesthetised, the portal vein exposed, and 16 ml/kg body weight of normal saline, with or without 10^{-5} mol/l human insulin, were injected. After 60 s, hindlimb muscles and epididymal fat were removed and immediately homogenised as described previously [28]. After centrifugation, the resultant supernatants were employed for immunoprecipitation or immunoblotting using the indicated antibodies as described previously [28]. Proteins were visualised with enhanced chemiluminescence and band intensities were quantified with a Molecular Imager GS-525 using Imaging Screen-CH (Bio-Rad). Bars depict means ± SE of the quantitated tyrosine phosphorylation bands, independently obtained in triplicate. Representative spots of PI(3)P are shown in the lower panels and bars depict means ± SE of PI 3-kinase activity measured in three independent assays. * $p<0.05$ compared with the control under the insulin-stimulated condition. IP, immunoprecipitation; IB, immunoblotting; pTyr, phosphotyrosine

adipocytes were incubated with 80 μmol/l BSO for 18 h [32]. It was reported that BSO treatment of adipocytes markedly decreases cellular glutathione levels and increases reactive oxygen species [15, 32]. Incubation with BSO did not affect the morphology or the viability of 3T3-L1 adipocytes (data not shown). Insulin-induced glucose uptake into 3T3-L1 adipocytes was decreased by 42.5% in BSO-treated cells (Fig. 4a). In these cells, insulin-induced GLUT4 translocation to the plasma membrane was impaired (Fig. 4b). Next, we determined insulin-induced IRS-1 phosphorylation and PI 3-kinase activation in whole cell lysates, the LDM fraction and the cytosol. As in rats, protein levels and insulin-induced tyrosine phosphorylations of IRS-1 and IRS-1-associated PI

3-kinase were unaffected by BSO treatment (Fig. 4c, upper panel). In control cells and in BSO-treated cells, p85 protein levels did not differ before versus after insulin stimulation. Next, we examined IRS-1 tyrosine phosphorylation and IRS-1 associated PI 3-kinase activity in the LDM fraction and the cytosol. While IRS-1 protein levels did not change after incubation with BSO, insulin-induced IRS-1 tyrosine phosphorylation in the LDM fraction was suppressed by BSO treatment (Fig. 4c, middle panel). The amount of p85 protein was increased in the LDM fraction and decreased in the cytosol after insulin stimulation, indicating that insulin induces p85 translocation from the cytosol to the LDM fraction in control cells. However, the p85 increase in the LDM fraction was clearly disrupted in BSO-treated cells (Fig. 4c, middle panel). In parallel, insulin-stimulation increased IRS-1-associated p85 protein levels and PI 3-kinase activity in the LDM fraction of control but not BSO-treated cells. Thus, BSO treatment disrupts insulin-induced IRS-1 phosphorylation in the LDM fraction and the subcellular redistribution of PI 3-kinase in 3T3-L1 adipocytes.

Inhibition of NF-κB activation improves BSO-induced insulin resistance. It is widely known that one potential target of oxidative stress is the activation of transcription factor NF-κB [33]. Oxidative stress and inflammatory cytokine stimulation reportedly activate upper kinase IκB kinase (IKK) which phosphorylates serine residues of IκB. The phosphorylated IκB is then subject to degradation, leading to translocation of NF-κB to the nucleus [34]. To investigate the role of NF-κB cascade activation in BSO-induced insulin re-
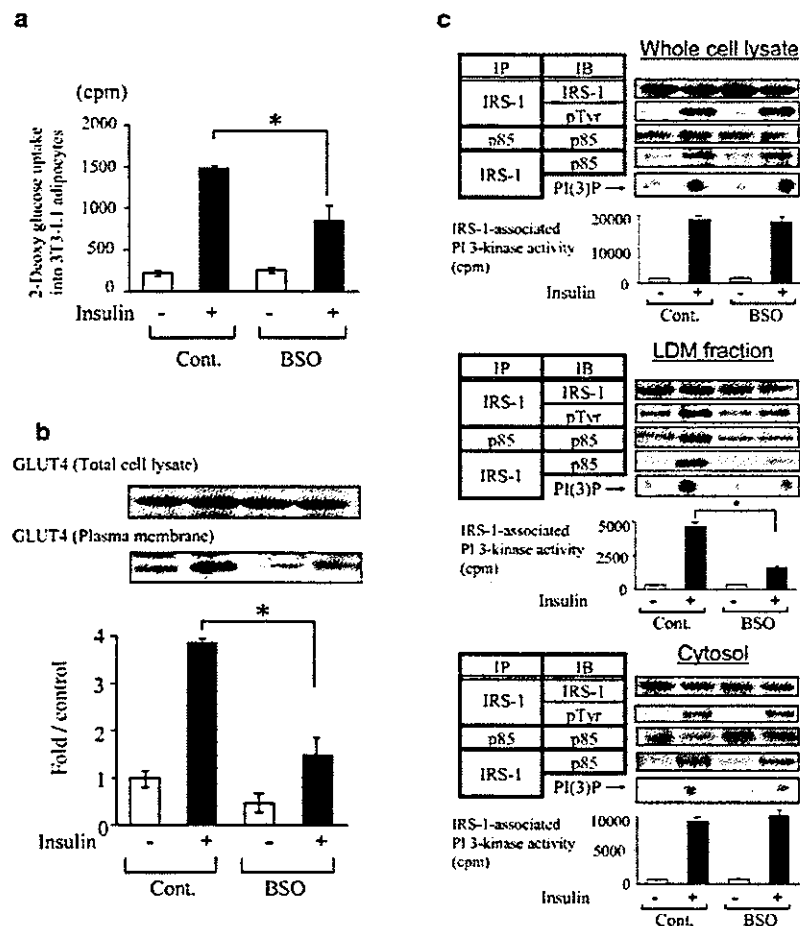
Fig. 4. Effects of BSO treatment on insulin action and insulin signalling in 3T3-L1 adipocytes. a. Insulin-induced 2-deoxy glucose uptake into 3T3-L1 adipocytes. 3T3-L1 adipocytes were serum-starved for 18 h, pre-incubated with or without 80 μmol/l BSO for 18 h. then incubated with or without 10^{-6} mol/l insulin for 15 min. 2-Deoxy glucose uptake was measured as described in Materials and methods. Bars depict means ± SE of results obtained independently in triplicate. * $p<0.05$ compared with the insulin-stimulated control. b. Recruitment of GLUT4 to the plasma membrane in 3T3-L1 adipocytes with or without BSO pretreatment. 3T3-L1 adipocytes were serum-starved for 18 h, pre-incubated with or without 80 μmol/l BSO for 18 h, then stimulated with or without 10^{-6} mol/l insulin for 15 min. Cells were fractionated as described previously [27]. The cell lysates and plasma membrane fraction were immunoblotted with anti-GLUT4 antibody. Representative immunoblots using anti-GLUT4 antibody are shown. Bars depict means ± SE of the quantitated bands of the plasma membrane fraction. independently obtained in triplicate. c. IRS-1 phosphorylation and IRS-1-associated PI 3-kinase in

whole cell lysates (upper panels), the LDM fraction (middle panels) and the cytosol (lower panels) in 3T3-L1. 3T3-L1 adipocytes were serum-starved for 18 h, pre-incubated with or without 80 μmol/l BSO for 18 h, then stimulated with or without 10^{-6} mol/l insulin for 15 min. Subcellular fractionation was performed as described in Materials and methods. The whole cell lysates and fractions were used for immunoprecipitation. immunoblotting and PI 3-kinase assay as described previously [28]. Proteins were visualised with enhanced chemiluminescence and band intensities were quantified with a Molecular Imager GS-525. Representative immunoblots are shown in the upper and middle panels and representative spots of PI(3)P, independently obtained in triplicate, are shown in the lower panel. Bars depict means ± SE of the quantitated spots of PI(3)P, indicating IRS-1-associated PI 3-kinase activity. independently obtained in triplicate. Cont., control 3T3-L1 adipocytes: BSO. pre-treated with 80 μmol/l BSO for 18 h. * $p<0.05$ compared with the control under the insulin-stimulated condition

sistance, we overexpressed the dominant negative mutant of IκB in 3T3-L1 adipocytes using adenovirus. This mutant, characterised by the substitution of two serine phosphorylation sites to alanine, is resistant to degradation and inhibits NF-κB-induced transcription.

In 3T3-L1 adipocytes, endogenous IκB was degraded by 5.8 pmol/l (equivalent to 10 ng/dl) of TNF-α or 80 μmol/l BSO pre-incubation for 18 h (Fig. 5a). However, the dominant negative IκB, overexpressed using adenovirus, was not degraded by these treat-
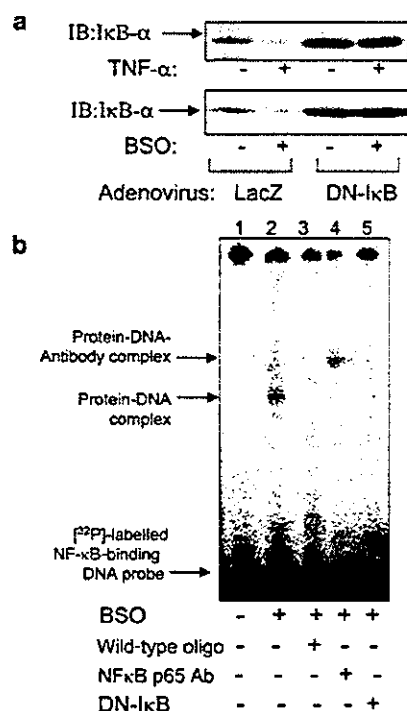
Fig. 5. Dominant negative mutant of IκB. a. Immunoblot of 3T3-L1 adipocytes overexpressing LacZ (control) and dominant negative mutant of I-κB adenoviruses. Representative immunoblots with anti-IκBα antibody of the cells incubated with 5.8 pmol/l (equivalent to 10 ng/ml) TNF-α and 80 μmol/l BSO for 18 h are shown in the upper and lower panels respectively. b. Gel mobility shift assay (GMSA). 3T3-L1 adipocytes were incubated with (lanes 2–5) or without (lane 1) 80 μmol/l BSO for 18 h. Dominant negative IκB was overexpressed in 3T3-L1 adipocytes (lane 5). Nuclear protein extracts from 3T3-L1 adipocytes were prepared as described in Materials and methods. For the GMSA, 10 μg of nuclear proteins were incubated in binding buffer with 3.5 pmol of double-stranded DNA oligonucleotide containing an NF-κB consensus binding sequence labelled with [^{32}P]-ATP using T4 polynucleotide kinase, for 30 min at 37 °C. For supershift analyses, monoclonal antibody against NF-κB p65 (NF-κB p65 Ab, lane 4) was separately pre-incubated with nuclear extracts at 4 °C for 20 min in a total volume of 16 μl of binding buffer, followed by incubation with 8 μl of ^{32}P-labelled oligonucleotide probe with and without a cold oligonucleotide probe (wild-type oligo, lane 3) at 4 °C for 20 min using a Nushift Kit (Geneka Biotechnology). Protein-DNA complexes were separated from the unbound DNA probe by electrophoresis through 5% polyacrylamide gels containing 1× Tris-glycine-EDTA buffer. The gel was dried and exposed to BAS2000 (Fujifilm, Tokyo, Japan). DN, dominant negative: IB, immunoblotting

ments (Fig. 5a). To investigate whether NF-κB binds to regulatory DNA elements, GMSA was performed using nuclear extracts of 3T3-L1 adipocytes. GMSA revealed nuclear protein extracts from BSO-treated 3T3-L1 adipocytes to contain activated NF-κB (Fig. 5b, lanes 1 and 2). The band shift was inhibited by unlabelled oligonucleotide corresponding to a

DNA-binding sequence (Fig. 5b, lane 3). In BSO-treated cells, the NF-κB-oligonucleotide complex underwent a supershift in the presence of antibodies against the p65 subunit of NF-κB, indicating that binding to the oligonucleotide is NF-κB-specific (Fig. 5b, lane 4). In 3T3-L1 adipocytes overexpressing the dominant negative IκB, the band shift was also inhibited (Fig. 5b, lane 5). These results suggest that BSO treatment induces NF-κB translocation and that the dominant negative IκB blocks NF-κB pathway activation.

We next examined the effect of the dominant negative IκB on BSO-induced insulin resistance. Insulin-induced glucose uptake was decreased by BSO treatment, while dominant negative IκB overexpression reversed this decrease (Fig. 6a). Reduction of insulin-induced GLUT4 translocation by BSO administration was also reversed by overexpression of the dominant negative IκB (Fig. 6b). BSO treatment decreased insulin-induced IRS-1 phosphorylation and IRS-1-associated p85 and PI 3-kinase activity in the LDM fraction (Fig. 6c, lower panels), but not in whole cell lysates (Fig. 6c, upper panels). However, overexpression of the dominant negative IκB reversed the BSO-induced decreases in IRS-1 phosphorylation and IRS-1-associated p85 and PI 3-kinase activity in the LDM fraction. These results suggest that oxidative stress induces insulin resistance by impairing the normal subcellular distribution of PI 3-kinase, and that the NF-κB pathway is involved in this process.

Discussion

In this study we employed BSO, a glutathione synthase inhibitor, to induce oxidative stress in rats and in 3T3-L1 adipocytes. BSO specifically inhibits the first step of glutathione synthesis and decreases glutathione, an important component of the antioxidant defence system [14]. In fact, we confirmed a decreased hepatic glutathione content and an increased plasma lipid hydroperoxide level, indicating increased oxidative stress in BSO-treated rats. Body weight was lower in BSO-treated rats than in controls, which is consistent with a previous report [35]. BSO-treated rats were apparently insulin-resistant, as demonstrated by a hyperinsulinaemic-euglycaemic clamp study and glucose transport assay using isolated skeletal muscle and adipocytes. These results strongly support the hypothesis that increased oxidative stress can lead to insulin resistance in vivo. Although fasting insulin levels were not elevated in BSO-treated rats as compared with controls, we found that among well-fed animals, insulin levels were significantly higher in BSO-treated rats than in controls. Data from the euglycaemic-hyperinsulinaemic clamp study, along with the observed glucose uptake into isolated tissues and insulin levels in well-fed animals, support the
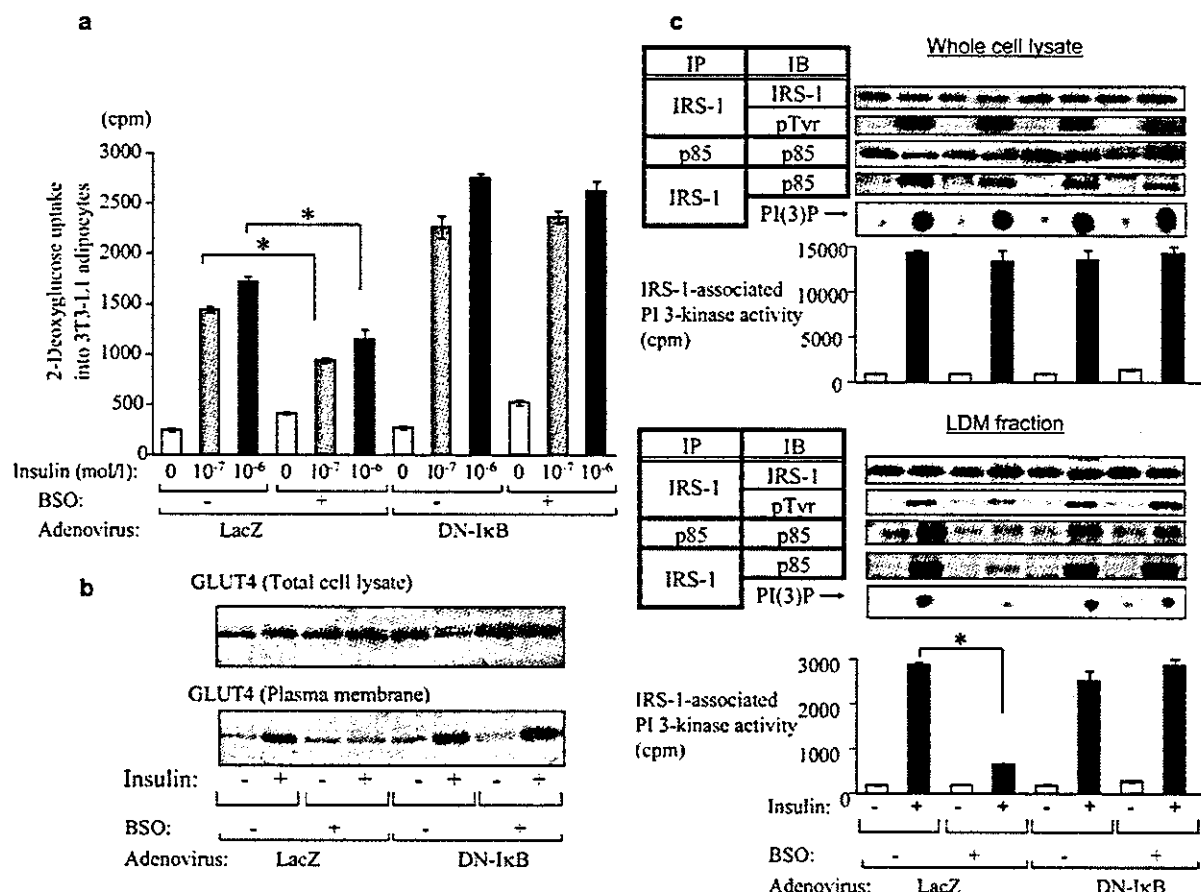
a

b   GLUT4 (Total cell lysate)

c

Fig. 6. Effect of dominant negative mutant of IκB on insulin action and insulin signalling in BSO-treated 3T3-L1 adipocytes. a. Insulin-induced 2-deoxy glucose uptake into 3T3-L1 adipocytes. Cells overexpressing LacZ (control) and the dominant negative (DN)-IκB adenovirus with or without 80 μmol/l BSO for 18 h were stimulated were stimulated with 0. 10^{-7} or 10^{-6} mol/l insulin for 15 min. Glucose uptake into 3T3-L1 adipocytes was assayed as described in Materials and methods. Bars depict means ± SE of results obtained independently in triplicate. ** $p<0.05$ compared to insulin-stimulated (10^{-7} and 10^{-6} mol/l respectively) control (non BSO-treated) cells. b. Recruitment of GLUT4 to the plasma membrane in 3T3-L1 adipocytes overexpressing LacZ and DN-IκB adenovirus with or without BSO pretreatment. The cell lysates and plasma membrane fraction were immunoblotted with anti-GLUT4 antibody. c. IRS-1 tyrosine phosphorylation. p85 protein amount and IRS-1-associated PI 3-kinase in whole cell lysates (upper panels) and the LDM fraction (lower panels) of 3T3-L1 adipocytes overexpressing LacZ and DN-IκB adenovirus with or without BSO pretreatment. 3T3-L1 adipocytes were serum-starved for 18 h, pre-incubated with or without 80 μmol/l BSO for 18 h, then stimulated with or without 10^{-6} mol/l insulin for 15 min. Representative immunoblots and representative spots of PI(3)P, independently obtained in triplicate, are shown and bars depict means ± SE of PI 3-kinase activity measured in three independent assays. * $p<0.05$ compared with insulin-stimulated control (non BSO-treated) cells. IB. immunoblotting; IP, immunoprecipitation

conclusion that BSO-treated rats are insulin-resistant. In our experiments, we did not observe the occurrence of overt diabetes with BSO administration, suggesting that this insulin resistance is relatively mild.

A previous report showed no significant difference between BSO-injected rats and controls in terms of insulin-stimulated glucose transport into skeletal muscle [15]. The results of their study contradict our present data demonstrating BSO-induced insulin resistance. We speculate that these different results are attributable to the doses of BSO administered. According to our water consumption data, intake of BSO in BSO-treated rats was approximately 3.5 mmol·kg⁻¹ body weight·day⁻¹ in the current study. This is a rather high dose compared with the previous report (2 mmol·kg⁻¹ body weight·day⁻¹) [15]. Also, the extent of the glutathione decrease was greater in our experiment than in the previous one. In addition, because the previous study did not employ the hyperinsulinaemic-euglycaemic clamp method [15], we believe our picture of insulin resistance in BSO-treated rats to be more accurate.

Insulin-induced IRS phosphorylation and PI 3-kinase activation constitute a critical step in insulin actions such as GLUT4 translocation and glucose uptake [36]. Most insulin-resistant models have been shown

to have impaired insulin-induced PI 3-kinase activation [28, 37, 38]. However, in the BSO-treated rats used in the current study, neither insulin-induced IRS tyrosine phosphorylation nor PI 3-kinase activation in whole tissue lysates of skeletal muscle and adipose tissue were impaired, despite the presence of insulin resistance. In addition, BSO treatment markedly impaired insulin-induced glucose uptake into 3T3-L1 adipocytes and GLUT4 translocation, while insulin-induced IRS-1 tyrosine phosphorylation and IRS-1-associated PI 3-kinase activation were unchanged in whole cell lysates of BSO-treated 3T3-L1 adipocytes. A previous report showed H_2O_2 exposure of 3T3-L1 adipocytes to inhibit insulin-induced glucose uptake, while having no effects on IRS-1 phosphorylation and PI 3-kinase activation [39]. Furthermore, we previously reported chronically angiotensin-II-infused rats, in which plasma lipid hydroperoxide levels were increased, to be highly insulin-resistant, although insulin-induced IRS-1 phosphorylation and PI 3-kinase activation in skeletal muscle and adipose tissue were not impaired [12]. Thus, insulin resistance with normal insulin-induced PI 3-kinase activation in the whole cell may be a common feature in the models with increased oxidative stress.

Regarding the molecular mechanism of this type of insulin resistance, we consider it necessary to examine the possibility of abnormalities in the subcellular distribution of PI 3-kinase. This is based on several reports showing IRS-1 phosphorylation and PI 3-kinase activation specifically in the LDM fraction, though not in whole cell lysates, to be important for insulin action [30, 31]. We speculate that the insulin-induced increase in IRS-1 phosphorylation in the LDM fraction leads to recruitment of the p85 subunit for PI 3-kinase to that fraction. Previous reports have shown that H_2O_2 exposure reduces IRS-1 tyrosine phosphorylation and PI 3-kinase activation in the LDM fraction in 3T3-L1 adipocytes [39, 40]. In the current study, insulin-induced IRS-1 tyrosine phosphorylation in the LDM fraction was demonstrated to be significantly decreased in both BSO-treated rat muscle and adipose tissues and in BSO-treated 3T3-L1 cells. We showed clearly that insulin induces p85 translocation from the cytosol to the LDM fraction in rat muscle, adipose tissue and 3T3-L1 cells and that BSO treatment disrupts this process. Taking our results and those of previous reports together, we consider this disruption of the normal subcellular redistribution of PI 3-kinase to be one of the important mechanisms underlying oxidative-stress-induced insulin resistance.

The activation of transcription factor NF-κB has been shown to be a target of oxidative stress [33]. For example, direct exposure to oxidants such as H_2O_2 activates NF-κB [41], while NF-κB activation can be inhibited by addition of antioxidants such as a vitamin E derivative [42] and lipoic acid [43]. To clarify the contribution of NF-κB cascade activation to oxida-

tive-stress-induced insulin resistance, we utilised the dominant negative IκB. This mutant is a degradation-resistant form of IκB that prevents NF-κB from translocating into the nucleus and is widely used to block cytokine-induced NF-κB activation [44]. Indeed, we confirmed that this mutant is not degraded by TNF-α and that BSO stimulation blocks NF-κB from translocating into the nucleus. Blocking the NF-κB cascade by overexpressing dominant negative IκB had a preventive effect against the decrease in insulin-induced glucose uptake and GLUT4 translocation caused by BSO treatment in 3T3-L1 adipocytes. We observed higher glucose uptake in dominant negative IκB-overexpressing cells than in LacZ control cells. We suggest a possible explanation: dominant negative IκB inhibits the effects of a small amount of inflammatory cytokines secreted by adipocytes. In addition, BSO-induced decreases in IRS-1 tyrosine phosphorylation in the LDM fraction and recruitment of PI 3-kinase to that fraction were also normalised. These results suggest that NF-κB activation is involved in the impaired subcellular redistribution of PI 3-kinase and the insulin resistance induced by BSO treatment.

The precise mechanism linking NF-κB activation and abnormal subcellular redistribution of PI 3-kinase remains unclear. One possible mechanism of inhibited insulin signalling involves NF-κB-activated transcription of inflammatory cytokines such as TNF-α and interleukin-6. NF-κB plays an important role in regulating inflammatory responses [45, 46] and activation of NF-κB may induce inappropriate inflammatory responses, possibly disrupting insulin signalling. Alternatively, PI 3-kinase activation is reportedly necessary for NF-κB activation [47, 48]. Aberrant NF-κB activation may disrupt the PI 3-kinase pathway via a negative feedback mechanism. An anti-inflammatory agent, salicylate, which stabilises IκB via inhibition of IKK and suppression of NF-κB activation, was shown to restore lipid-induced insulin resistance [49, 50]. Because IKK reportedly induces serine phosphorylation of IRS-1, it is possible that BSO activates IKK, resulting in down-regulation of IRS-1 tyrosine phosphorylation in the LDM fraction and impairment of PI 3-kinase recruitment to the LDM fraction.

In summary, our results suggest that oxidative stress induces insulin resistance by impairing insulin-induced IRS-1 phosphorylation in the LDM fraction and subcellular redistribution of PI 3-kinase, and that NF-κB activation is involved in this process. Our present study provides evidence that the NF-κB pathway plays a role in the pathogenesis of oxidative-stress-induced insulin resistance. Judging from our results and those of previous studies, strategies designed to limit inappropriate activation of NF-κB may be an effective approach to treating insulin resistance.

References

1. Betteridge DJ (2000) What is oxidative stress? Metabolism 49 [Suppl 1]:3–8

2. Reaven GM, Lithell H, Landsberg L (1996) Hypertension and associated metabolic abnormalities—the role of insulin resistance and the sympathoadrenal system. N Engl J Med 334:374–381

3. Tuck ML (1990) Metabolic considerations in hypertension. Am J Hypertens 3:355S–365S

4. Baynes JW (1991) Role of oxidative stress in development of complications in diabetes. Diabetes 40:405–412

5. Paolisso G, D'Amore A, Volpe C et al. (1994) Evidence for a relationship between oxidative stress and insulin action in non-insulin-dependent (type II) diabetic patients. Metabolism 43:1426–1429

6. Jones AF, Winkles JW, Jennings PE et al. (1988) Serum antioxidant activity in diabetes mellitus. Diabetes Res 7:89–92

7. Paolisso G, Di Maro G, Pizza G et al. (1992) Plasma GSH/GSSG affects glucose homeostasis in healthy subjects and non-insulin-dependent diabetics. Am J Physiol 263:E435–E440

8. Paolisso G, Balbi V, Volpe C et al. (1995) Metabolic benefits deriving from chronic vitamin C supplementation in aged non-insulin dependent diabetics. J Am Coll Nutr 14:387–392

9. Paolisso G, Di Maro G, Galzerano D et al. (1994) Pharmacological doses of vitamin E and insulin action in elderly subjects. Am J Clin Nutr 59:1291–1296

10. Rajagopalan S, Kurz S, Munzel T et al. (1996) Angiotensin II-mediated hypertension in the rat increases vascular superoxide production via membrane NADH/NADPH oxidase activation. Contribution to alterations of vasomotor tone. J Clin Invest 97:1916–1923

11. Schnackenberg CG, Wilcox CS (1999) Two-week administration of tempol attenuates both hypertension and renal excretion of 8-Iso prostaglandin f2alpha. Hypertension 33:424–428

12. Ogihara T, Asano T, Ando K et al. (2002) Angiotensin II-induced insulin resistance is associated with enhanced insulin signalling. Hypertension 40:872–879

13. Shimosawa T, Ogihara T, Matsui H et al. (2003) Deficiency of adrenomedullin induces insulin resistance by increasing oxidative stress. Hypertension 41:1080–1085

14. Meister A (1983) Selective modification of glutathione metabolism. Science 220:472–477

15. Khamaisi M, Kavel O, Rosenstock M et al. (2000) Effect of inhibition of glutathione synthesis on insulin action: in vivo and in vitro studies using buthionine sulfoximine. Biochem J 349:579–586

16. Vaziri ND, Wang XQ, Oveisi F, Rad B (2000) Induction of oxidative stress by glutathione depletion causes severe hypertension in normal rats. Hypertension 36:142–146

17. Ogihara T, Asano T, Ando K et al. (2001) Insulin resistance with enhanced insulin signalling in high-salt diet-fed rats. Diabetes 50:573–583

18. Yamamoto Y (1994) Chemiluminescence-based high-performance liquid chromatography assay of lipid hydroperoxides. Methods Enzymol 233:319–324

19. Anderson ME (1985) Determination of glutathione and glutathione disulfide in biological samples. Methods Enzymol 113:548–555

20. James DE, Burleigh KM, Kraegen EW (1986) In vivo glucose metabolism in individual tissues of the rat. Interaction between epinephrine and insulin. J Biol Chem 261:6366–6374

21. Hansen P, Gulve EA, Holloszy JO (1994) Suitability of 2-deoxyglucose for in vitro measurement of glucose transport activity in skeletal muscle. J Appl Physiol 76:979–985

22. Rodbell M (1964) Metabolism of isolated fat cells. I. Effects of hormones on glucose metabolism and lipolysis. J Biol Chem 239:375–380

23. Olefsky JM (1975) Effect of dexamethasone on insulin binding, glucose transport, and glucose oxidation of isolated rat adipocytes. J Clin Invest 56:1499–1508

24. Fujishiro M, Gotoh Y, Katagiri H et al. (2001) MKK6/3 and p38 MAPK pathway activation is not necessary for insulin-induced glucose uptake but regulates glucose transporter expression. J Biol Chem 276:19800–19806

25. Katagiri H, Asano T, Ishihara H et al. (1996) Overexpression of catalytic subunit p110alpha of phosphatidylinositol 3-kinase increases glucose transport activity with translocation of glucose transporters in 3T3-L1 adipocytes. J Biol Chem 271:16987–16990

26. Asano T, Kanda A, Katagiri H et al. (2000) p110beta is up-regulated during differentiation of 3T3-L1 cells and contributes to the highly insulin-responsive glucose transport activity. J Biol Chem 275:17671–17676

27. Satoh S, Nishimura H, Clark AE et al. (1993) Use of bis-mannose photolabel to elucidate insulin-regulated GLUT4 subcellular trafficking kinetics in rat adipose cells. Evidence that exocytosis is a critical site of hormone action. J Biol Chem 268:17820–17829

28. Anai M, Funaki M, Ogihara T et al. (1998) Altered expression levels and impaired steps in the pathway to phosphatidylinositol 3-kinase activation via insulin receptor substrates 1 and 2 in Zucker fatty rats. Diabetes 47:13–23

29. Sakoda H, Ogihara T, Anai M et al. (1999) No correlation of plasma cell 1 overexpression with insulin resistance in diabetic rats and 3T3-L1 adipocytes. Diabetes 48:1365–1371

30. Anai M, Ono H, Funaki M et al. (1998) Different subcellular distribution and regulation of expression of insulin receptor substrate (IRS)-3 from those of IRS-1 and IRS-2. J Biol Chem 273:29686–29692

31. Kriauciunas KM, Myers MG Jr, Kahn CR (2000) Cellular compartmentalization in insulin action: altered signaling by a lipid-modified IRS-1. Mol Cell Biol 20:6849–6859

32. Lu B, Ennis D, Lai R et al. (2001) Enhanced sensitivity of insulin-resistant adipocytes to vanadate is associated with oxidative stress and decreased reduction of vanadate (+5) to vanadyl (+4). J Biol Chem 276:35589–35598

33. Schreck R, Albermann K, Baeuerle PA (1992) Nuclear factor kappa B: an oxidative stress-responsive transcription factor of eukaryotic cells (a review). Free Radic Res Commun 17:221–237

34. Siebenlist U, Franzoso G, Brown K (1994) Structure, regulation and function of NF-kappa B. Annu Rev Cell Biol 10:405–455

35. Leeuwenburgh C, Ji LL (1995) Glutathione depletion in rested and exercised mice: biochemical consequence and adaptation. Arch Biochem Biophys 316:941–949

36. Czech MP (1995) Molecular actions of insulin on glucose transport. Annu Rev Nutr 15:441–471

37. Saad MJ, Folli F, Kahn JA, Kahn CR (1993) Modulation of insulin receptor, insulin receptor substrate-1, and phosphatidylinositol 3-kinase in liver and muscle of dexamethasone-treated rats. J Clin Invest 92:2065–2072

38. Cusi K, Maezono K, Osman A et al. (2000) Insulin resistance differentially affects the PI 3-kinase- and MAP kinase-mediated signalling in human muscle. J Clin Invest 105:311–320

39. Rudich A, Tirosh A, Potashnik R, Hemi R, Kanety H, Bashan N (1998) Prolonged oxidative stress impairs insulin-induced GLUT4 translocation in 3T3-L1 adipocytes. Diabetes 47:1562–1569

40. Tirosh A, Potashnik R, Bashan N, Rudich A (1999) Oxidative stress disrupts insulin-induced cellular redistribution of insulin receptor substrate-1 and phosphatidylinositol 3-kinase in 3T3-L1 adipocytes. A putative cellular mechanism for impaired protein kinase B activation and GLUT4 translocation. J Biol Chem 274:10595–10602

41. Schreck R, Rieber P, Baeuerle PA (1991) Reactive oxygen intermediates as apparently widely used messengers in the activation of the NF-kappa B transcription factor and HIV-1. EMBO J 10:2247–2258

42. Suzuki YJ, Packer L (1993) Inhibition of NF-kappa B activation by vitamin E derivatives. Biochem Biophys Res Commun 193:277–283

43. Sen CK, Packer L (1996) Antioxidant and redox regulation of gene transcription. FASEB J 10:709–720

44. Yamamoto Y, Gaynor RB (2001) Therapeutic potential of inhibition of the NF-kappaB pathway in the treatment of inflammation and cancer. J Clin Invest 107:135–142

45. Baeuerle PA, Henkel T (1994) Function and activation of NF-kappa B in the immune system. Annu Rev Immunol 12:141–179

46. Barnes PJ, Karin M (1997) Nuclear factor-kappaB: a pivotal transcription factor in chronic inflammatory diseases. N Engl J Med 336:1066–1071

47. Sizemore N, Leung S, Stark GR (1999) Activation of phosphatidylinositol 3-kinase in response to interleukin-1 leads to phosphorylation and activation of the NF-kappaB p65/RelA subunit. Mol Cell Biol 19:4798–4805

48. Reddy SA, Huang JH, Liao WS (2000) Phosphatidylinositol 3-kinase as a mediator of TNF-induced NF-kappa B activation. J Immunol 164:1355–1363

49. Kim JK, Kim YJ, Fillmore JJ et al. (2001) Prevention of fat-induced insulin resistance by salicylate. J Clin Invest 108:437–446

50. Yuan M, Konstantopoulos N, Lee J et al. (2001) Reversal of obesity- and diet-induced insulin resistance with salicylates or targeted disruption of Ikkbeta. Science 293:1673–1677

Atrial natriuretic peptide inhibits cardiomyocyte hypertrophy through mitogen-activated protein kinase phosphatase-1

Doubun Hayashi[a,b], Sumiyo Kudoh[a], Ichiro Shiojima[a], Yunzeng Zou[d], Koichiro Harada[a], Masaki Shimoyama[a], Yasushi Imai[a], Koshiro Monzen[a,b], Tsutomu Yamazaki[a,c], Yoshio Yazaki[e], Ryozo Nagai[a], Issei Komuro[d,*]

[a] Department of Cardiovascular Medicine, University of Tokyo Graduate School of Medicine, 7-3-1 Hongo, Bunkyo-ku, Tokyo 113-8655, Japan
[b] Department of Pharmacoepidemiology, University of Tokyo Graduate School of Medicine, 7-3-1 Hongo, Bunkyo-ku, Tokyo 113-8655, Japan
[c] Department of Clinical Bioinformatics, University of Tokyo Graduate School of Medicine, 7-3-1 Hongo, Bunkyo-ku, Tokyo 113-8655, Japan
[d] Department of Cardiovascular Science and Medicine, Chiba University Graduate School of Medicine, 1-8-1 Inohana, Chuo-ku, Chiba 260-8670, Japan
[e] International Medical Center of Japan, 1-21-1 Toyama, Shinjuku-ku, Tokyo 162-8655, Japan

Received 5 June 2004

Abstract

Cardiac hypertrophy is formed in response to hemodynamic overload. Although a variety of factors such as catecholamines, angiotensin II (AngII), and endothelin-1 (ET-1) have been reported to induce cardiac hypertrophy, little is known regarding the factors that inhibit the development of cardiac hypertrophy. Production of atrial natriuretic peptide (ANP) is increased in the hypertrophied heart and ANP has recently been reported to inhibit the growth of various cell types. We therefore examined whether ANP inhibits the development of cardiac hypertrophy. Pretreatment of cultured cardiomyocytes with ANP inhibited the AngII- or ET-1-induced increase in the cell size and the protein synthesis. ANP also inhibited the AngII- or ET-1-induced hypertrophic responses such as activation of mitogen-activated protein kinase (MAPK) and induction of immediate early response genes and fetal type genes. To determine how ANP inhibits cardiomyocyte hypertrophy, we examined the mechanism of ANP-induced suppression of the MAPK activation. ANP strongly induced expression of MAPK phosphatase-1 (MKP-1) and overexpression of *MKP-1* inhibited AngII- or ET-1-induced hypertrophic responses. These growth-inhibitory actions of ANP were mimicked by a cyclic GMP analog 8-bromo-cyclic GMP. Taken together, ANP directly inhibits the growth factor-induced cardiomyocyte hypertrophy at least partly via induction of MKP-1. Our present study suggests that the formation of cardiac hypertrophy is regulated not only by positive but by negative factors in response to hemodynamic load.
© 2004 Elsevier Inc. All rights reserved.

Keywords: Angiotensin II; Atrial natriuretic peptide; Cardiac hypertrophy; Cardiomyocyte; Cyclic GMP; Endothelin-1; Growth factor; MAPK phosphatase-1; Mitogen-activated protein kinase; Vasoactive peptide

Since cardiac myocytes virtually lose their proliferative ability soon after birth, they respond to external stimuli not by increasing the cell number but by increasing the individual cell volume, called hypertrophy. Although cardiac hypertrophy has been considered to

be a beneficial adaptive response of the heart to the increased workload, the hypertrophic heart often leads to dilated cardiomyopathy and eventually causes congestive heart failure after sustained overload [1]. Recent clinical studies have demonstrated that the increased ventricular mass is an independent risk factor for cardiac morbidity and mortality [2]. Therefore, it has become even more important to elucidate the molecular mechanism of how cardiac hypertrophy is formed.

* Corresponding author. Fax: +81 43 226 2557.
  E-mail address: komuro-tky@umin.ac.jp (I. Komuro).

A variety of factors have been implicated in the pathogenesis of cardiac hypertrophy [3]. Vasoactive peptides such as angiotensin II (AngII) [3–7] and endothelin-1 (ET-1) [8,9] have been reported to induce cardiomyocyte hypertrophy by autocrine or paracrine mechanisms. These factors are produced and secreted in the heart in response to the increased overload and induce cardiomyocyte hypertrophy. Antagonists of these factors effectively inhibit the load-induced cardiomyocyte hypertrophy [6–9]. The intracellular signaling pathways initiated by these growth factors and the resultant hypertrophic responses in cardiomyocytes have also been intensively investigated. AngII and ET-1 activate various protein kinases including protein kinase C and the mitogen-activated protein kinase (MAPK) family. Activation of these protein kinases induces expression of many specific genes [10–12] and an increase in protein synthesis [12].

Among the genes that are upregulated in the hypertrophied heart, atrial natriuretic peptide (ANP) has unique features. ANP reduces the hemodynamic load as a potent vasorelaxing and diuretic–natriuretic peptide, which indirectly inhibits the development of cardiac hypertrophy [13]. In addition to the indirect effects of ANP via hemodynamics, ANP has recently been reported to have direct growth-inhibitory effects in various cell types such as vascular smooth muscle cells, glomerular mesangial cells, endothelial cells, cardiac fibroblasts, and astrocytes [14–19]. In these cells, 8-bromo-cyclic GMP (8-Br-cGMP), a cell permeable analog of cyclic GMP (cGMP), mimicked the effects of ANP, indicating that the growth-inhibitory effects of ANP are dependent on cGMP. Furthermore, it has recently been reported that ANP induces expression of MAPK phosphatase-1 (MKP-1) [20]. MKP-1 is a dual serine/threonine and tyrosine phosphatase and specifically inactivates MAPK family members [21]. Overexpression of MKP-1 blocks the MAPK-dependent gene expression and inhibits cell proliferation [22–24]. These observations suggest that ANP may exert its inhibitory effects on cell growth through inactivation of MAPK family members by induction of MKP-1. Three members of the MAPK family, the extracellular signal-regulated kinases (ERKs), the c-Jun NH_2-terminal kinases/stress-activated protein kinases (JNKs/SAPKs), and p38MAPKs, have been shown to be activated by hypertrophic stimuli in cardiac myocytes and have been implicated in the development of cardiac hypertrophy [25–30].

In the present study, we examined whether ANP has direct inhibitory effects on growth factor-induced cardiomyocyte hypertrophy. Pretreatment with ANP suppressed the growth factor-induced increase in the cell volume and the protein synthesis of cardiomyocytes. ANP also inhibited hypertrophic responses such as activation of MAPK and induction of immediate early

response genes and fetal type genes. In addition, ANP strongly induced expression of MKP-1 in cardiac myocytes and overexpression of *MKP-1* suppressed AngII-induced gene expressions. These results suggest that anti-hypertrophic effects of ANP are, at least in part, mediated by inactivation of MAPK via induction of MKP-1. These inhibitory actions of ANP were mimicked by a cGMP analog, 8-Br-cGMP.

Materials and methods

Cell culture. Primary cultures of cardiomyocytes were prepared from ventricles of 1-day-old Wistar rats as described previously [6]. Except for the reporter gene assay, cells were plated at a field density of 1×10^3 cells/mm^2 on 35-mm culture dishes and cultured in DMEM with 10% FBS for the first 24 h, and then the culture medium was changed to DMEM containing 0.1% FBS. After 48 h of serum starvation, cardiomyocytes were stimulated by various agents. For transfection and reporter gene assay, cells were plated at the same density, and subjected to transfection after 24 h of culture in DMEM with 10% FBS.

Immunofluorescence. Immunostaining of cardiomyocytes with MF20, a monoclonal antibody against sarcomeric myosin heavy chain (MHC), was performed as described previously [7]. An anti-mouse immunoglobulin G conjugated with tetramethyl rhodamine isothiocyanate was used as the secondary antibody. The cell size of cardiomyocytes was measured by directly tracing the stained areas on a photograph.

[^{3}H]Phenylalanine incorporation. Protein synthesis was assessed by measuring the [^{3}H]phenylalanine incorporation as previously described [7]. Cardiac myocytes were cultured for 2 days without serum and then incubated for 24 h with AngII, ET-1 or vehicle. [^{3}H]Phenylalanine (1.0 μCi/ml) was added 3 h before the harvest. Cells were washed three times with ice-cold phosphate-buffered saline (PBS), incubated 30 min with 1 ml of 10% trichloroacetic acid, and washed twice with PBS. Precipitates were solubilized for 30 min in 800 μl of 1 N NaOH, and radioactivity was measured by liquid scintillation spectroscopy.

Northern blot analysis. Total cellular RNA was extracted from cardiac myocytes by acid-guanidine phenol–chloroform method. Ten micrograms of total RNA was size-fractionated by 1.2% agarose gels and transferred to nylon membranes. Northern blot analyses were performed using the *c-fos* and *ANP* cDNA as probes as described previously [26,31]. The cDNA of rat *MKP-1* was isolated by the polymerase chain reaction method with a pair of primers corresponding to the amino acids 174–181 and 342–349.

Transfection and reporter gene assay. The luciferase reporter plasmids (3 μg/dish) containing ~1800 bp 5' flanking region of the *brain natriuretic peptide (BNP)* gene (a kind gift from Dr. Y. Saito, Kyoto) were transiently transfected into cultured cardiac myocytes using standard calcium phosphate method. Cells were washed with PBS at 12 h after transfection and culture medium was changed to the medium containing 0.1% FBS. After 24 h of serum starvation, cells were treated with various reagents. Cells were harvested at 48 h after stimulation in 150 μl of extraction buffer (100 mM tricine, 10 mM MgSO$_4$, 2 mM EDTA, pH 7.8, and 1 mM dithiothreitol) and luciferase activities were measured by Berthold Lumat LB9501 luminometer. Next, 1 μg of luciferase reporter plasmids containing the human *c-fos* promoter